frontiers | Frontiers in Marine Science

ORIGINAL RESEARCH
published: 28 July 2022
doi: 10.3389/fmars.2022.823793

Interannual Variations of $D^{14}C_{TOC}$ and Elemental Contents in the Laminated Sediments of the Santa Barbara Basin During the Past 200 Years

Hong-Chun Li[1,2], Yiwei Chang[1], William M. Berelson[3], Meixun Zhao[2], Satabdi Misra[1] and Tzu-Tsen Shen[1]*

[1]Department of Geosciences, National Taiwan University, Taipei, Taiwan, [2]Frontiers Science Center for Deep Ocean Multispheres and Earth System, and Key Laboratory of Marine Chemistry Theory and Technology, Ministry of Education, Ocean University of China, Qingdao, China, [3]Department of Earth Sciences, University of Southern California, Los Angeles, CA, United States

OPEN ACCESS

Edited by:
Núria Casacuberta, ETH Zürich, Switzerland

Reviewed by:
Fasong Yuan, Cleveland State University, United States
Amzad Hussain Laskar, Physical Research Laboratory, India
Haiyan Jin, Ministry of Natural Resources, China

***Correspondence:**
Hong-Chun Li
hcli1960@ntu.edu.tw

Specialty section:
This article was submitted to Marine Biogeochemistry, a section of the journal Frontiers in Marine Science

Received: *28 November 2021*
Accepted: *15 June 2022*
Published: *28 July 2022*

Citation:
Li H-C, Chang Y, Berelson WM, Zhao M, Misra S and Shen T-T (2022) Interannual Variations of $D^{14}C_{TOC}$ and Elemental Contents in the Laminated Sediments of the Santa Barbara Basin During the Past 200 Years. Front. Mar. Sci. 9:823793. doi: 10.3389/fmars.2022.823793

A 51-cm core (SBB-8-2012) from the depo-center of Santa Barbara Basin (SBB), California has been dated by ^{210}Pb dating and varve counting, spanning a depositional history during 1815-2011 CE. A total of 89 AMS ^{14}C measurements on samples from 66 horizons, including animal cartilage, shell and total organic carbon (TOC) in the sediments show apparent ^{14}C ages between 500 and 4000 yr BP. Among these AMS dates, $D^{14}C$ values measured in 78 samples from 62 horizons vary in the range of -64.3‰ to -383.8‰. The $^{14}C_{TOC}$ ages much older than predicted from our sedimentation model are influenced by the input of terrigenous sediments, changes in ocean circulation, biological input and carbon remineralization. Three strong old $^{14}C_{TOC}$ excursions at 1964~69, 1884~87 and 1819~21 CE indicate higher old carbon input caused by some unusual events (e.g., oil spill, flood event and earthquake). On multi-decadal timescales, the $D^{14}C_{TOC}$ shifts in three zones were mainly caused by changes in fossil carbon emission from the seafloor, fraction of marine productivity to terrigenous input of organic carbon (OC) and the atmospheric nuclear bomb testing input of ^{14}C into the SBB. On interannual to decadal timescales, variations of $D^{14}C_{TOC}$ correspond to El Niño-Southern Oscillation effects. During the La Niña period, stronger upwelling and northerly California Current bring nutrient-enriched water into SBB and lead to higher productivity hence more marine OC with higher $D^{14}C_{TOC}$. In addition, reduced terrigenous input of OC with lower $D^{14}C$ under less coastal rainfall during La Niña could further elevate the $D^{14}C_{TOC}$. Lower scanning XRF (K+Ti)/2 (indicating lower terrigenous input), higher scanning XRF Sr/Ti as well as acid-leachable elements (reflecting higher biogenic components), and higher $D^{14}C_{TOC}$ occur during La Niña. During the El Niño period, the phenomena are opposite. Spectrum analyses of the Southern Oscillation Index (SOI) and the $D^{14}C_{TOC}$ as well as the comparison of SOI and SBB-8-2012 records support our scenarios.

Keywords: $^{14}C_{TOC}$ variation, elemental content, laminated sediment, Santa Barbara basin, El Niño/La Niña, iTRAX XRF scan corer, Icp-oes analysis, acid-leachable elements

1 INTRODUCTION

With anoxic conditions on the bottom of Santa Barbara Basin (SBB) offshore of California, laminated sediments have regularly been used to reconstruct high-resolution paleoclimate records (Kennett and Brassell, 1992; Schimmelmann and Lange, 1992; Kennett and Ingram, 1995; Heusser, 1998; Schimmelmann et al., 1998; Schimmelmann et al., 2003; Robert, 2004; Schimmelmann et al., 2006; Barron and Bukry, 2010; Barron et al., 2015; Sarno et al., 2020), and natural disaster signals such as earthquake and flooding events (Schimmelmann et al., 2001; Schimmelmann et al., 2013; Hendy et al., 2015; Du et al., 2018). Numerous investigations of SBB water column, sediment trap and sediment core analyses have been conducted on carbon and nitrogen cycles (e.g., Andrew and Peter, 1977; Pisias, 1978; Lynn and Simpson, 1990; Schimmelmann and Tegner, 1991; Thunell, 1998; Emmer and Thunell, 2000; Thunell, 2003; Tems et al., 2015; Davis et al., 2019; White et al., 2019), biological productivity and chemical conditions in the basin and their linkage to climate and water mixing (e.g., Browne, 1994; Gorsline, 1996; Weinheimer and Cayan, 1997; Warrick et al., 2005; Lund, 2011; Berelson et al., 2019; Napier et al., 2019).

Terrestrial organic carbon input by episodic discharge events from the mountain river systems can survive in coastal processing near Santa Barbara Channel (Kolpack and Drake, 1984; Thunell et al., 1995; Schimmelmann and Lange, 1996). The organic carbon (OC) can be rapidly transported to low-oxygen seafloor sediments in SBB where remineralization is less efficient (Sarno et al., 2020). Due to restricted circulation below the basin sills, oxygen supply to the bottom water of SBB is limited, so a suboxic environment exists at a depth below 480 m (Li et al., 2009). The anoxic condition in SBB is also attributed to the emission of methane and crude oil from oil seeps in the region contribute reduced carbon. For instance, the Coal Oil Point seep field, located at near shore of SBB, is one of the largest natural submarine hydrocarbon emission areas in the world (Allen and Mikolaj, 1970; Hornafius et al., 1999; Valentine et al., 2010) and likely contributes fossil carbon input to SBB. With those exogenous carbons (old and dead carbons), the ^{14}C reservoir age in SBB is older than that of the average world ocean and varies over time (Kennett et al., 1997). Several groups have studied the ΔR (regional differences in the radiocarbon age between sea-surface water and average world surface water, McFadgen and Manning, 1990) in SBB *via* different methods. Ingram and Southon (1996) used mollusc shell ^{14}C measurements in SBB and found the ΔR of 233±60 years for the Santa Barbara Channel region, close to the average for the coast of California. Kennett et al. (1997) used ^{14}C dates of marine shell and charcoal pairs from finely stratified archaeological deposits at Daisy Cave and Cave of the Chimneys located on San Miguel Island and concluded that the ΔR varied from -360 to 310 years during the Holocene. Hendy et al. (2013) compared 49 mixed planktonic foraminiferal carbonate and 20 terrigenous organic carbon (such as wood, leaves, seeds or charcoal) ^{14}C dates to the varve chronology in a sediment core from SBB and found that the ΔR between 80 and 350 years during the past 2000 years. Therefore, it is necessary to further understand the factors that affect the ^{14}C reservoir ages of SBB.

The ^{14}C reservoir age in SBB is related to oceanic circulation, upwelling of the Pacific deep water, El Niño–Southern Oscillation (ENSO) and Pacific Decadal Oscillation (PDO) (Kennett et al., 1997; Hendy et al., 2013; Du et al., 2018). This is because the regional rainfall of southern California, oceanic circulation and upwelling along the southern California coast are strongly influenced by summer insolation, ENSO and PDO (Kennett et al., 1997 and references therein; Lynn and Bograd, 2002; Jacox et al., 2015). During the warm phases of ENSO (El Niño state) and PDO, rainfall and river discharge increase around SBB, supplying more terrestrial sediments to the depo-center of SBB (Shipe et al., 2002; Warrick and Farnsworth, 2009; Hendy et al., 2015). During this period, the southerly flow of California Counter Current brings warm, nutrient-depleted water from the equatorial Pacific to suppress northerly flow and nutrient-rich California Current as well as upwelling, resulting in low marine productivity (Bray et al., 1999; Bograd and Lynn, 2001; Bograd et al., 2002; Venrick, 2012). On the other hand, increase (decrease) in summer insolation results in warmer air masses over western North America, enhancing (reducing) northwesterly winds and upwelling intensity along the California coast (Kennett et al., 1997). However, up to date, there is no annual to interannual variability of ^{14}C reservoir age in the SBB sediment records to provide evidence for the above scenario. We address this topic in our work here. Furthermore, Hendy et al. (2015) used a 250-yr varved core (SPR0901-04BC) from SBB to identify droughts and floods related to ENSO impact by using changes in elemental contents measured with scanning X-ray fluorescence (XRF), inductively coupled plasma atomic emission spectrometer (ICP-AES) and inductively coupled plasma mass spectrometer (ICPMS). They have found that siliciclastic sediments containing the elements Ti, Fe, K, Al, Si, and Rb have higher scanning XRF intensities during El Niño events and positive (warm) phases of PDO, and biogenic indicators such as Ca/Ti, Sr/Ti and Br/Cl have lower values during El Niño events and negative (cool) phases of the PDO (Hendy et al., 2015). Are we able to reproduce such conclusions?

This study presents results of ^{14}C measurement, scanning XRF elemental content and acid-leachable elemental concentration of the sediments in a 51-cm core from the depo-center of SBB. The core was dated by ^{210}Pb and varve counting. The refined chronology of the core indicates that the sedimentary history of the core covers 1815-2011 CE. The high-resolution (3-yr) $D^{14}C_{TOC}$ record combined with the elemental records allows us to understand sedimentary variations under influence of climatic and oceanographic changes. In this paper, we will discuss the influencing factors of the $D^{14}C_{TOC}$ (i.e., apparent ^{14}C age of total organic carbon) in SBB sediments. The outputs of our results benefit not only the understanding of the variation of the ^{14}C reservoir effect in the Santa Barbara Channel, but also the reconstruction of paleoclimate and paleo-ENSO changes.

2 MATERIALS AND METHODS

2.1 SBB-8-2012 Core and Sampling

SBB-8-2012 (34°17'N, 120°03'W) was a 51-cm long core collected by a multi-core device in the depo center of the Santa Barbara Basin at a water depth of 580 m by the research team of Prof. William Berelson at the University of Southern California (USC) in August 2012 (**Figure 1**). The core was split in half and kept in a cold room at 4°C in the Department of Earth Sciences at USC. Half of the core was transported to the Department of Geosciences at the National Taiwan University (NTU) in 2015. During the transportation, the sediments below 12.5 cm separated from the section above, perhaps caused by differential drying due to changes in grain size, density and organic content, etc. (**Figure 2A**). This shrinkage resulted in a 3-cm gap in the core. Therefore, we have to calibrate the scanned and sampling depths back to the original depths (**Figure 2B**). Owing to changes in moisture content of the core during the storage (more than 3 years) at USC and transportation from USC to NTU, the water content of the sediments was not measured.

The half core was scanned by an iTRAX core scanner at NTU. After the scan, the core was subsampled at 1-cm interval for ^{210}Pb dating, then subsampled at 2~3-mm interval (roughly 4 samples within one centimeter) with a stainless steel knife for fine resolution analyses. During the sampling, any visible shells, plant or animal remains in the sediments, were picked up individually for ^{14}C dating purposes. Only less than 1/2 of the sediments throughout the half core were taken at NTU, and the rest was sent back to USC where δ^{13}C, δ^{15}N and C/N of the organic matter were planned to be analyzed. Due to the limited amount of subsamples, we did not measure grain size, bulk density and TOC for every sample. All sediment samples were freeze-dried by a Freeze vacuum dryer (model EYELA FDU-1200), then ground and mixed well. The samples were placed in plastic bags and stored in a refrigerator at 8°C until analysis.

2.2 iTRAX XRF Core Scan

The iTRAX XRF scan was performed at NTU with an iTRAX core scanner (Li et al., 2015; Löwemark and Itrax operators, 2019). The core with smooth and flat surface was placed in the XRF scanner which contains a digital optical RBG image, a digital radiographic image, and a μ-XRF elemental profile. The scanning condition was using a Mo tube set at 30 kV and 30 mA, a sampling interval of 200 μm and an exposure time of 40 s. For duplicating checks, the core was scanned twice along two parallel tracks which are 3-mm apart. Elements including Fe, Ca, Sr, K, Ti, Mn, Rb, Zn, Ni, Cu, Si, S, Cl, V, Cr, Co, Y, Zr, Nb, Pd, Cd, In, Sn, Sb, Al, Ba and Pb were measured, but only part of the elements provided meaningful results. The criteria for selecting meaningful data are: 1. The maximum intensity of an element during the entire scan should be greater than 200 counts per second (cps); and 2. The correlation coefficient (R^2) of the element along the two duplicated tracks should be greater than 0.6. With such criteria, only Fe, Ca, Sr, K, Ti, Mn, Rb, Zn, Ni, Cu, Si, Cl, Y, Zr and Pb provide meaningful results.

2.3 ^{210}Pb Dating

^{210}Pb dating method was originally established by Goldberg (1963). ^{210}Pb profile of a sedimentary sequence can be described by the following equation:

$$^{210}Pb = {}^{210}Pb_0 * e^{-\lambda t} = {}^{210}Pb_0 * e^{-\lambda * D/SR} \quad (1)$$

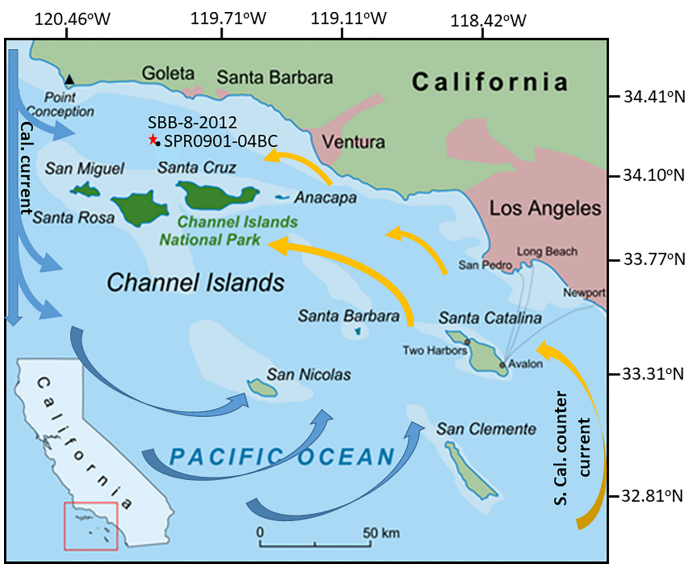

FIGURE 1 | Location map of the study area. The red star shows the location of core SBB-8-2012 site in Santa Barbara Basin and the black dot indicates core SPR0901-04BC location of Hendy et al. (2015). Blue arrows present cold and nutrient-rich current from north, whereas the orange arrows reflect warm and nutrient-depleted current from south.

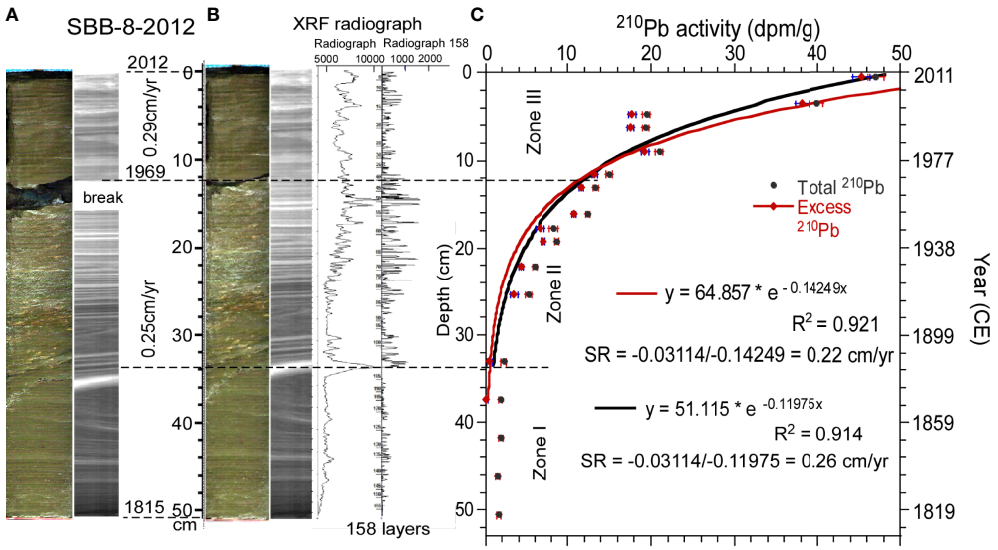

FIGURE 2 | Picture, X-ray radiograph, lamination counting and ^{210}Pb dating of Core SBB-8-2012. **(A)** Core photo during XRF scanning and sampling. The breaking gap between 12cm and 13cm was formed during the transportation from USA to Taiwan. **(B)** Core photo after adjusted the depths to remove the breaking gap. The lighter bands in the radiograph reflect the layers with less density. The brightest band at 34 cm indicates an organic rich layer in which all elemental contents by iTRAX XRF scanning are low. **(C)** ^{210}Pb profile of the core. The constructed ages are shown on the right-hand side of the plot. The red curve and black curve fittings are using different ending depths of excess ^{210}Pb, which result different sedimentation rates.

where $^{210}Pb_0$ and ^{210}Pb are the initial activity and activity at a past time (or depth), respectively. λ is the decay constant of ^{210}Pb (0.0311 yr^{-1}). D stands for depth in a sedimentary profile. SR refers to the linear sedimentation rate. Taking logarithms to Eqn. (1), we have:

$$Ln^{210}Pb = Ln^{210}Pb_0 - \lambda * D / SR \quad (2)$$

If $^{210}Pb_0$ and SR are relatively constant, the slope of Ln ^{210}Pb — D should yield a linear sedimentation rate SR. This is the fundamental concept of ^{210}Pb dating.

Since the subsample of the core was not enough for our gamma spectrometry, ^{210}Po alpha method was used for the ^{210}Pb dating (Baskaran and Iliffe, 1993; Baskaran and Krishnamurthy, 1993; Li et al., 1996; Paulsen et al., 2003; Li et al., 2011; Kuo et al., 2011; Yin et al., 2014; Zhao et al., 2015; Yin et al., 2017; Zhao et al., 2017a; Yin et al., 2019). As a daughter product of ^{210}Pb decay, ^{210}Po has a half-life of 138.38 days. Hence, within a couple of years, ^{210}Pb and ^{210}Po reach secular equilibrium. The ^{210}Po activity equals that of ^{210}Pb in the measured samples.

A total of 17 horizons from the 1-cm interval samples were selected throughout the core for ^{210}Po dating in the AMS ^{14}C dating Lab at NTU (the NTUAMS Lab) (**Table 1**). Each dry sample of 0.3~0.5 g was spiked with ^{209}Po in a Teflon beaker and dissolved by aqua regia on a hot plate at 95°C overnight. The sample solution was evaporated to dryness, then added 4N HCl to dissolve residues. The sample solution was transferred into a centrifuge tube for the removal of any detritus. After centrifuge, the supernatant was poured back into the Teflon beaker and evaporated to dryness. Ten ml 1.0 N HCl was added into the Teflon beaker to dissolve the sample. Then, transfer the sample into a 50-ml plastic centrifuge tube. Ascorbic acid powder was added to the solution until it became clear (yellow color would be disappeared) in order to remove the influence of Fe. A silver disc (0.8 cm in diameter) was placed at the bottom of the centrifuge tube. The Po in the sample was self-precipitated onto the silver disc within an 80°C water bath for 6 hours. After washing with deionized water (DIW), the silver disc was counted for ^{210}Po (5304 keV) and ^{209}Po (4884 keV) by an ORTEC alpha spectrometer at NTU. **Table 1** lists the ^{210}Po dating results.

2.4 AMS ^{14}C Dating

Accelerator mass spectrometry (AMS) ^{14}C dating was performed in the NTUAMS Lab at NTU with a 1.0 MV Tandetron Model 4110 BO AMS. About 50~100 mg of dry sediments were weighted for TOC ^{14}C dating and acid-leachable element analysis. The sample was dissolved in 15 ml 0.5N HCl for removal of carbonates. Using pH paper to check the solution, when pH<3, all inorganic carbons were dissolved by the acid leaching. Centrifuging the sample and washing the residue with DIW, and collecting the supernatant for inductively coupled plasma-optical emission spectrometer (ICP-OES) analysis. The residue was dried at 50°C. The TOC of the dried residue sample was oxidized into CO_2 under 850°C. Then, the purified CO_2 was made into graphite following the description in Yang et al. (2017) and Zhao et al. (2017b). Six samples (samples with # symbol in **Table 2**) were used a different acidification treatment for AMS ^{14}C dating. For these samples, the sample was placed in a reaction vessel on a vacuum line for CO_2 collection. The sediment sample in

TABLE 1 | ^{210}Pb dating results. The excess ^{210}Pb is determined by the ^{210}Po at each layer subtracting the mean ^{210}Po value averaged from the four ^{210}Po values in the deep part.

Sample ID	Weight (g)	Depth (cm)	^{210}Po (dpm/g)	Excess ^{210}Pb (dpm/g)
SBB-8 0-1	0.37	0.5	47.06±0.98	45.35±0.98
SBB-8 3-4	0.30	3.5	39.89±0.81	38.18±0.81
SBB-8 4-5.5	0.56	4.8	19.46±0.48	17.75±0.48
SBB-8 5.5-7	0.48	6.3	19.30±0.40	17.59±0.40
SBB-8 8-10	0.54	9.0	21.00±0.47	19.29±0.47
SBB-8 10-12	0.49	11.5	14.95±0.37	13.24±0.37
SBB-8 15.5-17	0.51	13.1	13.35±0.30	11.64±0.30
SBB-8 18-20	0.53	16.1	12.44±0.27	10.73±0.27
SBB-8 20-21	0.31	17.7	8.31±0.49	6.60±0.49
SBB-8 21-22.5	0.64	19.1	8.69±0.26	6.98±0.26
SBB-8 24-25	0.37	22.0	5.96±0.25	4.25±0.25
SBB-8 27-28	0.31	25.4	5.16±0.41	3.45±0.41
SBB-8 34-35	0.30	33.1	2.19±0.32	0.48±0.32
SBB-8 38-39	0.37	37.4	1.82±0.22	0.11±0.22
SBB-8 42-43	0.30	41.8	1.88±0.28	
SBB-8 46-47	0.35	46.1	1.50±0.23	
SBB-8 50-51	0.47	50.6	1.64±0.25	

the reaction vessel was reacted with 1 ml of 100% H_3PO_4 on the vacuum line. After the CO_2 extraction of the total inorganic carbon (TIC) in the sample was done, the collected CO_2 was made into graphite for ^{14}C dating following the description in Zhao et al. (2015). The residue in the reaction vessel was collected into a centrifuge tube and washed by DIW. After centrifuging, the residue was dried at 50°C. The TOC in the dried residue was processed for ^{14}C dating according to the above description. In so doing, we can compare the ^{14}C results of TOC and TIC from the same sediment samples. For every batch of the samples, at least three oxalic acid standards (OXII, SRM 4990C), three organic carbon backgrounds (BKG, made from anthracite), three carbonate backgrounds (NTUB, made from Upper Devonian limestone) and two known-age inter-comparison samples (IRI, distributed by the University of Glasgow) were processed in the same procedures and measured with the sample targets.

One sample is animal cartilage (looks like a fish spine). This sample was just cleaned with DIW, and placed into a 9-mm size quartz tube with pre-combusted CuO powder. The tube was sealed under a vacuum of 10^{-5} mbar, and then combusted for 6 h at 850°C in a muffle furnace. The carbon from this sample came from mainly organic components, so that we classified its ^{14}C dating as TOC ^{14}C dating. There are four TIC ^{14}C dates of sediment samples (samples with @ symbol in **Table 2**) and two ^{14}C dates of a conch shell. These samples had the same procedure for TIC ^{14}C dating as described earlier for the samples with # symbol.

The AMS measured both ^{14}C/^{12}C and ^{13}C/^{12}C ratios on all graphite targets. The AMS measurement was setup for four cycles and each cycle contained 50 blocks (30 seconds for every block). When the ^{14}C counts in a measurement cycle reached 40,000, the counting would stop. Therefore, ^{14}C counts of OXII are normally greater than 40,000, with a statistic error<0.5%. In general, the precision of the ^{14}C dating at the NTUAMS Lab is better than 3%.

The percent modern carbon (pMC) was calculated by background corrected and ^{13}C/^{12}C fractionation corrected ^{14}C/^{12}C ratios between sample and OXII following the concept and definition in Stuiver and Polach (1977); Kim et al. (2001) and Stenström et al. (2011):

$$pMC = \frac{\left(\frac{^{14}C}{^{12}C}\right)_{s,bkg,corr}}{\left(\frac{^{14}C}{^{12}C}\right)_{oxII,bkg,corr}} \times 100\% = \frac{\left(\frac{^{14}C}{^{12}C}\right)_{s-bkg} \times \left(1 - \frac{2\times(25+\delta(^{13}C)_s}{1000}\right)}{\left(\frac{^{14}C}{^{12}C}\right)_{oxII-bkg} \times \left(1 - \frac{2\times(25-18)}{1000}\right)} \times 100\% \quad (3)$$

where ^{14}C/^{12}C with subscripts of s,bkg,corr and oxII,bkg,corr represents background and δ^{13}C corrected ^{14}C/^{12}C value of sample and standard, respectively. The ^{14}C/^{12}C with subscripts of s-bkg and oxII-bkg refers to background corrected ^{14}C/^{12}C value of sample and standard, respectively. Note that δ^{13}C correction for AMS ^{14}C dating must use ^{13}C/^{12}C measurement on the AMS, but not δ^{13}C measured by an isotope ratio mass spectrometry (IRMS) because the isotopic fractionation is different for the two processes. The δ^{13}C value of OXII is -17.88‰ (round to -18‰). δ^{13}C value of a sample [$\delta(^{13}$C)s] determined by the AMS was calculated by equation (4):

$$\delta(^{13}C)_S = \left[\frac{\left(\frac{^{13}C}{^{12}C}\right)_S \times \left(1 - \frac{18}{1000}\right)}{\left(\frac{^{13}C}{^{12}C}\right)_{OXII}} - 1\right] \times 1000‰ \quad (4)$$

TABLE 2 | All AMS data uncertainties have 2σ error.

Lab code (NTUAMS-)	Sample ID	Type	Depth (cm)	pMC (%)	$D^{14}C$ (‰)	^{14}C age (year BP)	Calendar year by ^{210}Pb dating (CE)
2772-2	SBB 0-0.8	TOC	0.4	93.57±1.21	-64.3±0.8	534±104	2011
4125-2	SBB 0-1cm TIC	TIC	0.5	85.17±0.96	-148.3±1.7	1289±90	2010
3830	SBB 1.1cm	TOC	1.1	90.58±0.91	-94.2±0.9	795±81	2008
2773	SBB 2-2.2	TOC	2.1	90.74±1.14	-92.6±1.2	781±101	2005
3831	SBB 3.1cm	TOC	3.1	90.10±0.91	-99.0±1.0	838±81	2001
3603	SBB 3-4cm TIC	TIC	3.5	74.07±1.17	-259.3±4.1	2411±127	2000
3802	SBB 3-4cm TOC	TOC	3.5	88.09±0.93	-119.1±1.3	1019±85	2000
2774	SBB 4-4.2	TOC	4.1	92.60±1.18	-74.0±0.9	617±102	1998
3832	SBB 5.1cm	TOC	5.1	88.50±0.93	-115.0±1.2	982±84	1994
4192	SBB 6.1 cm	TOC	6.1	83.69±0.84	-163.1±1.6	1430±80	1991
3604	SBB 5.5-7cm TIC	TIC	6.75	82.03±0.89	-179.7±1.9	1591±87	1990
3803	SBB 5.5-7cm TOC	TOC#	6.75	88.28±0.92	-117.2±1.2	1002±83	1990
3833	SBB 7.1cm	TOC	7.1	86.76±0.90	-132.4±1.4	1141±83	1988
4194	SBB 8.1cm	TOC	8.1	86.96±0.98	-130.4±1.5	1122±90	1984
2776-1	SBB 8-8.2cm	TOC	8.1	88.98±0.58	-110.2±0.7	938±53	1984
3834	SBB 9.1cm	TOC	9.1	88.51±1.00	-114.9±1.3	981±91	1981
2777-1	SBB 10-10.2cm	TOC	10.1	91.53±0.59	-84.7±0.5	711±52	1977
2777-2	SBB 10-10.2cm	TOC	10.1	92.42±0.58	-75.8±0.5	633±51	1977
4126	SBB 10-11cm TIC	TIC	10.5	85.21±0.69	-147.9±1.2	1286±65	1974
3870	SBB 11.1cm	TOC	11.1	89.63±0.77	-103.7±0.9	879±69	1974
3871	SBB 12.1cm	TOC	12.1	88.99±0.76	-110.1±0.9	937±68	1970
2778-1	SBB 12.2-12.4cm	TOC	12.3	86.90±0.56	-131.0±0.8	1128±51	1970
2778-2	SBB 12.2-12.4cm	TOC	12.3	86.57±0.61	-134.3±0.9	1159±56	1970
2779-1	SBB 15.8-16.0cm	TOC	15.9	85.25±0.58	-147.5±1.0	1282±54	1968
4053	SBB 16.9cm	TOC	16.9	71.84±0.76	-281.6±3.0	2657±85	1964
4015	SBB 17-18cm TIC	TIC	17.5	89.53±0.74	-104.7±0.9	888±66	1962
3872	SBB 18.1cm	TOC	18.1	89.71±0.67	-102.9±0.8	872±60	1959
2781-1	SBB 19-19.2cm	TOC	19.1	87.97±0.52	-120.3±0.7	1029±47	1954
3873	SBB 20.1cm	TOC	20.1	86.28±0.67	-137.2±1.1	1185±63	1950
2782	SBB 21-21.2cm	TOC	21.1	85.28±0.51	-147.2±0.9	1279±48	1945
2783	SBB 23-23.2cm	TOC	23.1	82.11±0.51	-178.9±1.1	1583±50	1937
3874	SBB 24.1cm	TOC	24.1	85.02±0.65	-149.8±1.2	1304±62	1932
2681-1	SBB 25-25.2cm	TOC	25.1	84.39±0.73	-156.1±1.3	1363±69	1928
2681-2	SBB 25-25.2cm	TOC	25.1	84.64±0.73	-153.6±1.3	1340±69	1928
3072	SBB-25.5CM	TOC	25.5	82.15±0.65	-178.5±1.4	1580±63	1926
3073	SBB-26.5CM	TOC	26.5	81.33±0.63	-186.7±1.4	1660±62	1922
2680-1	SBB 27-27.2cm	TOC	27.1	81.26±0.71	-187.4±1.6	1667±71	1919
2680-2	SBB 27-27.2cm	TOC	27.1	80.19±0.69	-198.1±1.7	1774±69	1919
3234	SBB 28.2~28.4	TOC	28.4	77.83±0.43	-221.7±1.2	2014±45	1914
3235-1	SBB 28.6~28.8	TOC	28.7	79.79±0.37	-202.1±0.9	1814±37	1912
3235-2	SBB 28.6~28.8	TOC	28.7	80.12±0.38	-198.8±0.9	1781±38	1912
2679-1	SBB 29-29.2cm	TOC	29.1	83.47±0.74	-165.3±1.5	1452±72	1910
2679-2	SBB 29-29.2cm	TOC	29.1	83.11±0.74	-168.9±1.5	1487±71	1910
3074	SBB-29.5CM	TOC	29.5	83.15±0.71	-168.5±1.4	1482±69	1909
3236-2	SBB 30.2~30.4	TOC	30.3	80.50±0.40	-195.0±1.0	1743±40	1905
3237-2	SBB 30.6~30.8	TOC	30.7	80.58±0.47	-194.2±1.1	1734±47	1903
2678-1	SBB 31-31.2cm	TOC	31.1	83.41±0.72	-165.9±1.4	1457±69	1902
2678-2	SBB 31-31.2cm	TOC	31.1	82.24±0.79	-177.6±1.7	1570±77	1902
3238-1	SBB 31.6-31.8	TOC	31.4	79.39±0.53	-206.1±1.4	1854±54	1899
3238-2	SBB 31.6-31.8	TOC	31.4	80.79±0.52	-192.1±1.2	1713±52	1899
3239-1	SBB 32.2-32.4	TOC	32.3	75.28±0.72	-247.2±2.4	2281±77	1896
3239-2	SBB 32.2-32.4	TOC	32.3	79.48±0.52	-205.2±1.3	1845±52	1896
3240	SBB 32.6-32-8	TOC	32.4	78.24±0.57	-217.6±1.6	1972±59	1895
2677-1	SBB 33-33.2cm	TOC	33.1	80.66±0.75	-193.4±1.8	1726±75	1893
2677-2	SBB 33-33.2cm	TOC	33.1	81.31±0.73	-186.9±1.7	1662±72	1893
3241	SBB 33.8-34.0	TOC	33.9	79.23±0.56	-207.7±1.5	1871±56	1889
3605	SBB 34-35cm TIC	TIC	34.5	79.68±0.99	-203.2±2.5	1825±100	1888
3801	SBB 34-35cm TOC	TOC#	34.5	76.62±0.80	-233.8±2.4	2139±83	1888
3242-1	SBB 34.6-34.8	TOC	34.7	78.45±0.51	-215.5±1.4	1949±52	1886
3242-2	SBB 34.6-34.8	TOC	34.7	78.14±0.52	-218.6±1.5	1981±54	1886
2676-1	SBB 35-35.2cm	TOC	35.1	69.24±0.67	-307.6±3.0	2952±77	1884
2676-2	SBB 35-35.2cm	TOC	35.1	68.79±0.64	-312.1±2.9	3006±75	1884

(Continued)

TABLE 2 | Continued

Lab code (NTUAMS-)	Sample ID	Type	Depth (cm)	pMC (%)	$D^{14}C$ (‰)	^{14}C age (year BP)	Calendar year by ^{210}Pb dating (CE)
2675	SBB 35.5-37 TOC	Cartilage	36.25	93.78±0.83	-62.2±0.6	516±71	1881
3075	SBB-36.5CM	TOC	36.5	79.06±0.61	-209.4±1.6	1888±62	1878
3606	SBB 38-39cm	TIC	38.5	73.53±0.89	-264.7±3.2	2469±97	1869
3804	SBB 38-39cm TOC	TOC	38.5	75.06±0.77	-249.4±2.6	2304±83	1869
3077	SBB-38.5CM	TOC	38.5	76.04±0.62	-239.6±2.0	2201±66	1869
2674-1	SBB 38.5cm Conch	Shell	38.5	88.51±0.80	-114.9±1.0	980±73	1869
2674-2	SBB 38.5cm Conch	Shell	38.5	88.18±0.80	-118.2±1.1	1010±73	1869
3078	SBB-39.1CM	TOC	39.1	79.91±0.62	-200.9±1.6	1802±63	1867
3079	SBB-39.5CM	TOC	39.5	77.64±0.62	-223.6±1.8	2033±64	1865
3080	SBB-40.1CM	TOC	40.1	80.06±0.62	-199.4±1.5	1786±62	1862
3875	SBB 41.1cm	TOC	41.1	77.62±0.69	-223.8±2.0	2035±71	1858
3450	SBB 42.1cm	TOC	42.1	72.71±0.80	-272.9±3.0	2560±85	1854
3876	SBB 43.1cm	TOC	43.1	78.44±0.61	-215.6±1.7	1951±62	1849
4054	SBB 43.9cm	TOC	43.9	73.10±0.75	-269.0±2.8	2517±83	1846
4193	SBB 44.1cm TIC	TOC	44.1	72.56±0.64	-274.4±2.4	2577±71	1845
3557	SBB 44.1cm TOC	TOC#	44.1	70.67±0.58	-293.3±2.4	2788±65	1845
3877	SBB 45.1cm	TOC	45.1	80.25±0.70	-197.5±1.7	1768±70	1840
3452	SBB 46.1cm	TOC	46.1	75.55±0.83	-244.5±2.7	2252±75	1836
3783	SBB 46-47cm TIC	TIC	46.5	77.47±0.94	-225.3±2.7	2051±98	1834
3828	SBB 46-47cm TOC	TOC#	46.5	77.28±0.79	-227.2±2.3	2070±82	1834
3878	SBB 47.1cm	TOC	47.1	78.57±0.70	-214.3±1.9	1937±71	1832
3453	SBB 48.1cm	TOC	48.1	74.81±0.85	-251.9±2.9	2332±78	1827
4055	SBB 49.1cm	TOC	49.1	69.66±0.80	-303.4±3.5	2904±92	1823
4056	SBB 49.9cm	TOC	49.9	61.62±0.65	-383.8±4.1	3889±85	1819
3784	SBB 50-51cm TIC	TIC	50.5	77.58±1.02	-224.2±2.9	2040±105	1817
3829	SBB 50-51cm TOC	TOC#	50.5	74.18±0.78	-258.2±2.7	2400±85	1817
3454	SBB 50.9cm	TOC	50.9	73.88±0.81	-261.2±2.9	2432±81	1815

All total organic carbon (TOC) samples are treated by 0.5N HCl, except samples with # symbol. The samples with # symbol were extracted CO_2 by H_3PO_4 first, then the samples were used for TOC dating. In the NTUAMS Lab code, -1 or -2 following the code indicates that the sample has enough CO_2 to split two aliquots for making graphite target.

By Eqns. (3) and (4), pMC is obtained with background and $\delta^{13}C$ (to -25‰) corrections. $D^{14}C$ and apparent age of the sample were calculated by Eqns. (5) and (6), respectively:

$$D^{14}C = \left(\frac{pMC}{100} - 1 \right) \times 1000‰ \quad (5)$$

$$\mathrm{Age}\left(yr\,BP \right) = -8033 \times \ln\left(\frac{pMC}{100} \right) \quad (6)$$

We do not use $\Delta^{14}C$ value which represents the activity ratio of a sample (A_s) to the atmospheric CO_2 (A_{abs}) without age correction (Stenström et al., 2011), whereas A_{abs} refers to the hypothetical specific activity of atmospheric carbon of year 1950. The relationship between $\Delta^{14}C$ and $D^{14}C$ can be described by Eqn. (7):

$$\Delta^{14}C = \left(D^{14}C + 10^{-3} \right) e^{(y-1950)/8267} + 10^{-3} \quad (7)$$

where y in Eqn. (7) is the measurement year. As this study does not focus on the ^{14}C variation in the atmosphere, there is no need to use $\Delta^{14}C$. Furthermore, in order to show the age difference between ^{14}C and ^{210}Pb results, we also calculated the ^{14}C ages. As these ^{14}C dates contain old carbon influences, there is no meaning to provide the calibration dates. We will use the apparent (measured) ^{14}C dates and $D^{14}C$ values for discussion. All $D^{14}C$ values and ^{14}C dates are listed in **Table 2**.

2.5 Acid-Leachable Elemental Analysis

A total of 72 horizons from the core were subsampled for acid-leachable elemental measurement. The sample weight ranged from 48.45 mg to 325.15 mg with an average and standard deviation of 96.34±51.11 mg (n = 72), implying a very limited sample amount. These samples were leached by 15 ml 0.5N HCl. This procedure is not only for the removal of inorganic carbon during TOC ^{14}C dating, but also for the dissolution of elements that exist in authigenic (precipitated in water column) minerals such as carbonates (both inorganically precipitated in surface water and in biological shells) and oxides as well as absorbed on the particle surface. This procedure does not affect organic components and detrital phases in the sediments. The elements in the solution are considered as an active portion which reflects chemical conditions and productivity in the water column. The sample solution was measured by a PerkinElmer (PE) Optima 8000DV ICP-OES in the NTUAMS Lab. Elements of Ca, Fe, Mg, Ti, Al, Sr, Ba, Mn, Zn, Cr, Cu and Pb were selected for analysis. The concentrations of all elements measured by ICP-OES need to be calculated by the standard curves made from different concentrations of the standard solutions. The standard solutions were made from ICP multi-element standard IV (Certipur® 1.11255.0100) produced by *Marck KaGaA*, Germany. During the ICP-OES runs, the standard solutions were measured with the sample solutions multiple times. The correlation coefficient (R^2) of intensity-concentration relationship for each element is normally greater than 0.98. For the first three batches of ICP-OES

TABLE 3 | Acid-leachable (0.5 N HCl) elemental concentrations in the sediments of Core SBB-8-2012.

Depth (cm)	Age (CE)	Ca	Fe	Mg	Al	Sr	Mn
0.4	2011	31.48	13.81	11.78	2.86	267.44	131.97
1.1	2008	35.73	28.91	10.89	5.75	281.80	184.49
1.5	2007	11.61	20.49	11.91	6.44	201.76	348.50
2.1	2005	13.97	6.00	3.63	2.27	92.73	89.37
2.5	2003	27.74	15.91	9.00	6.37	164.02	177.86
3.1	2001	38.85	65.99	24.93	32.86	274.71	390.35
3.5	2000	17.84	22.94	9.24	6.95	115.28	203.96
4.1	1998	20.49	21.08	6.58	3.38	119.60	130.86
4.5	1996	32.10	27.85	9.45	5.76	201.96	200.17
5.1	1994	91.33	45.94	21.2	35.08	496.00	342.86
5.5	1993	36.52	19.37	8.93	6.63	203.82	239.92
6.1	1991	31.42	11.69	8.01	3.42	210.53	169.25
6.5	1990	39.80	19.69	9.88	7.70	213.82	223.12
7.1	1988	133.63	83.82	42.62	37.43	778.70	670.28
7.5	1986	38.04	17.93	9.95	6.70	200.02	179.61
8.1	1984	31.79	10.29	7.16	3.35	170.13	102.08
8.5	1983	42.17	21.02	10.27	8.24	231.19	234.47
9.1	1981	114.21	56.27	28.62	23.99	661.25	465.58
9.5	1979	33.06	22.61	11.37	8.83	191.30	264.72
10.1	1977	29.80	19.18	7.84	3.86	165.90	149.85
10.5	1976	36.32	22.24	9.38	5.87	200.87	197.25
11.1	1974	48.03	17.73	7.44	3.63	265.32	94.24
11.5	1972	37.94	22.09	11.14	7.52	217.73	208.84
12.1	1970	44.90	10.48	6.76	3.70	267.26	77.96
12.3	1970	31.46	8.49	6.09	3.17	184.74	122.16
12.7	1968	24.66	7.63	5.55	3.12	141.33	117.77
13.8	1964	58.53	35.49	14.56	9.33	335.37	226.32
14	1963	18.98	12.42	5.67	2.89	111.06	112.88
15.1	1959	27.32	18.52	6.50	3.68	150.79	99.09
16.2	1954	10.22	3.87	3.25	1.58	81.76	95.27
17.3	1950	33.22	15.49	8.92	5.21	185.75	158.07
18.4	1945	23.63	11.17	5.43	3.20	122.78	100.06
20.6	1937	16.72	11.27	5.87	4.50	119.15	116.60
21.7	1932	39.49	14.02	7.27	4.44	224.64	127.90
22.8	1928	20.03	12.20	6.77	3.84	119.48	162.15
23.2	1926	20.40	22.01	10.73	8.82	131.83	239.61
23.9	1924	26.96	27.42	11.34	10.38	163.00	262.51
24.3	1922	34.10	28.62	10.99	9.06	193.13	244.20
24.9	1919	24.58	18.68	8.91	7.08	161.04	194.98
25.4	1917	36.48	28.14	12.5	10.4	182.72	253.78
26	1915	12.47	17.21	7.20	6.25	75.73	160.29
26.5	1913	26.01	26.60	9.50	8.76	151.70	205.88
27.1	1910	18.74	9.59	5.10	3.50	98.95	112.93
28.2	1906	14.53	12.15	5.81	4.59	91.20	157.52
29.3	1902	15.57	12.93	5.85	4.02	101.60	166.67
30.4	1897	23.24	29.89	9.50	9.96	136.92	216.41
31.5	1893	27.38	14.64	8.08	5.67	164.89	183.51
32.6	1889	25.03	21.91	10.67	9.35	154.85	226.90
33	1887	12.23	13.58	6.49	5.70	80.10	147.45
33.7	1884	19.11	17.46	10.98	7.42	121.35	206.02
34.1	1882	16.15	18.05	9.05	7.16	105.42	202.65
34.6	1881	28.70	25.90	11.97	9.25	160.09	244.21
35.2	1878	27.27	12.05	7.73	3.97	140.41	135.50
35.9	1875	14.45	14.66	8.92	3.59	91.42	147.14
36.3	1874	12.75	14.47	9.57	3.20	84.57	116.20
37	1871	8.98	9.46	6.19	2.36	60.95	124.48
37.4	1869	21.43	14.52	8.17	4.38	112.57	136.65
38.1	1867	26.8	11.78	7.80	5.86	197.02	148.66
38.5	1865	36.82	13.01	8.88	4.60	186.75	133.95
39.2	1862	40.36	11.08	8.16	4.04	199.70	124.88
40.3	1858	45.87	9.90	7.72	3.98	233.71	99.45
41.4	1854	29.21	4.49	5.42	2.50	218.52	105.91
42.5	1849	45.20	9.61	8.33	3.74	227.23	90.73
43.3	1846	87.51	25.4	18.46	10.00	450.54	229.61

(Continued)

TABLE 3 | Continued

Depth (cm)	Age (CE)	Ca	Fe	Mg	Al	Sr	Mn
43.5	1845	28.74	5.01	6.07	2.79	192.40	115.88
44.6	1840	52.37	11.81	8.50	3.52	256.73	112.35
45.7	1836	34.70	6.55	7.62	3.07	207.10	131.39
46.8	1832	48.89	9.49	7.20	3.27	255.56	99.41
47.9	1827	48.29	5.51	6.63	2.79	292.07	120.30
49	1823	72.04	15.91	12.22	5.46	341.97	187.91
49.9	1819	46.99	13.73	8.72	5.48	285.52	185.34
51	1815	36.16	6.04	6.51	2.61	230.67	107.08

The unit for Ca, Fe, Mg and Al is g/Kg, whereas the unit for Sr and Mn is mg/Kg.

runs, 1 ml sample solution was diluted with 9 ml 0.5N HNO_3. However, some heavy metal elements such as Zn and Pb were not detectable. In the final run, 5 ml sample solution was diluted with 5 ml 0.5N HNO_3. But, the intensity of Ti, Ba, Zn, Cr, Cu and Pb were still low, and might contain some memorial effects from the 100 ppm (mg/L) standard solution during the measurement. Therefore, the measurements of those elemental concentrations may not be reliable. For Ca, Fe, Mg, Al, Sr and Mn which have high concentrations and sensitivities for the ICP-OES measurements, their results should be reliable for discussion. For these elements, the detection limit is about 1 ppb with precision normally better than 2%. **Table 3** lists the concentrations of the acid-leachable elements.

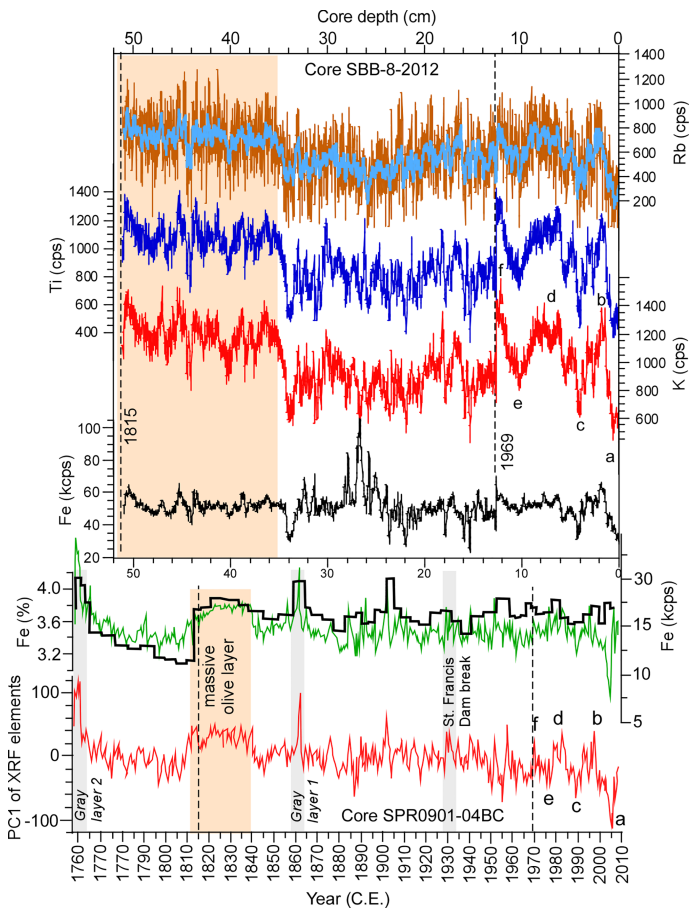

FIGURE 3 | Comparison of scanned XRF elemental contents between Core SBB-8-2012 (this study) and Core SPR0901-04BC (Hendy et al., 2015) from the Santa Barbara Basin. Curves for Fe, K and Ti are 9-point running average of the raw data (roughly monthly resolution). For Rb, the orange curve represents the raw data, and the light blue curve stands for 9-point running average of the raw data.

3 RESULTS

3.1 Sediment Features of the Core

The sediments of the core are generally fine clay in size with an average TOC of 3.82% and dry bulk density of 0.85 g/cm^3. The core sediments show clear laminations on the X-ray radiograph (**Figure 2B**) with lighter bands reflecting less dense, organic-rich layers. An outstanding light band appears at 34-35 cm depth. The sediments of the core can be classified into three zones: Zone I (35-51 cm depth), the sediments had higher density with thinner lamination. Zone II (12-34 cm depth), the sediments became less dense (increasing light intensity in the radiograph) with clear laminations. Between 26 cm and 27 cm depth, a visible brownish band existed, which was probably caused by a high concentration of Fe oxide (scanning XRF results in **Figure 3** show the evidence). In this zone, the sediments contain some white materials (light spots shown in **Figure 2B**), but they are not carbonates because acid-leachable elements especially Ca, Mg and Sr do not show high concentrations. Zone III (0-12 cm depth), the sediments in this zone have darker color and thick laminations. As we will discuss them in later sections, the criteria for dividing the core into 3 zones are based on four reasons: (1) changes in the $D^{14}C$ trend; (2) changes in the elemental contents; (3) two outstanding depositional layers: one is at 12-13 cm and the other is at 34-35 cm; and (4) changes in the sedimentary features including color and thickness of laminations as described above.

3.2 Chronology of the Core

The radiograph generated by the iTRAX core scanner allows us to count laminations of the sediments using a computer software called ItraxPlot (https://www.raddec.com/software-itraxplot.php). The counting result indicates that the sediment core has 158 contrast (a dark and light couplet) layers (**Figure 2B**). If the laminations are annual, then the sediment core contains 158 years with a mean sedimentation rate of 0.32 cm/yr. However, the varve counting may not be accurate and its annual assumption may not be valid. Thus, we applied ^{210}Pb dating to the core.

The total ^{210}Pb activity in the core ranges from 47.06 to 1.50 dpm/g, with an exponential decay trend from the surface toward to bottom (**Figure 2C**). The ^{210}Pb activities at 4-7 cm depth are slightly low, perhaps due to lower initial ^{210}Pb activity in the input materials. The ^{210}Pb activities below 37 cm depth (ranging from 1.5 to 1.88 dpm/g) are relatively invariant, reflecting supported ^{210}Pb activity. Hence, we use the average of the four deepest ^{210}Pb activities to represent the supported ^{210}Pb which is 1.71 dpm/g. The excess ^{210}Pb value of each layer equals the total ^{210}Pb value subtracting the supported ^{210}Pb (**Table 1**). Using exponential fitting of the excess ^{210}Pb with depth, we get an equation of $y = 64.857^{*}e^{-0.14249x}$. The sedimentation rate (SR) is 0.22 cm/y. Based on this sedimentation rate, the 51-cm long core would cover about 230 years of depositional history, which is significantly longer than the varve counting result (158 years). In fact, ^{210}Pb dating has about 5% uncertainty, especially depending on the determination of the ending point of the excess ^{210}Pb. For example, if we decide the ending point of excess ^{210}Pb is at 33-cm depth instead of 37-cm, the fitting curve (black line in **Figure 2C**) provides a sedimentation rate of 0.26 cm/yr, which gives 196-year depositional history. Nevertheless, based on the ^{210}Pb dating, the sedimentation rate is around 0.22~0.26 cm/yr. In addition, since the ^{210}Pb dating assumes a constant sedimentation rate and constant initial ^{210}Pb concentration, the conditions may not be valid. Therefore, we need to further refine the chronology of the core.

Hendy et al. (2015) published elemental contents measured by both scanning XRF and ICPMS analyses of bulk elemental concentrations in the sediments of Core SPR0901-04BC (34°16.7' N, 120°02.49' W, 588 m) which had a close location to our core (**Figure 1**). This core covers a sedimentary history of 1755-2008 CE. The chronology of this core was determined by "the distinctive changes in the sedimentary fabric of SBB cores created by the strong El Niño events of 1941, 1957, 1983, and 1997", "the gray layer at 1761 AD, the turbidite at 1811 AD, and the bioturbated *Macoma* event at 1841 AD" and varve chronology (Hendy et al., 2015). Although this core did not have direct radiometric dating, the historic events and varve chronology recorded in the sediments made its chronology with an error of ±2 years around those controlling points (Hendy et al., 2015). Comparison of the scanning XRF results between Core SPR0901-04BC and Core SBB-8-2012 can help us to refine the chronology of SBB-8-2012.

In **Figure 3**, the lower panel shows the profiles of the first principal component (PC1, which explains 45.5% of the elemental variance in the core) of scanning XRF elements which include Al, Fe, K, Rb, Si and Ti) and Fe variations measured by both scanning XRF and ICP-MS during 1755-2008 CE (Hendy et al., 2015). The upper panel displays the profiles of Fe, K, Rb and Ti measured by scanning XRF in Core SBB-8-2012 with depth. First of all, scanning XRF measurement of the elements should be the total elemental content of all types including organic, authigenic and detrital phases in the materials within a few hundred micrometers (μm) (the penetration depth of the X-ray). Since scanning XRF is semi-quantitative in nature, the XRF elemental content cannot represent the total elemental concentration measured by ICP-MS in the sediment, and the latter should be the true elemental concentration. Secondly, the XRF scan has a very high-resolution (200 μm sampling interval), whereas the ICP-MS measurement has much lower resolution in general (1 cm sampling interval for the lower panel in **Figure 3**). Thirdly, once a core opened to air, oxidation of the surface sediments will allow some oxidation of reduced compounds (e.g., FeS can be oxidized to produce Fe_2O_3). Therefore, for the scanning XRF elements which can be influenced by the oxidation (e.g., Ca and Fe), discrepancies between XRF and ICP-MS trends are understandable. However, the variation trends of Fe, K, Ti, Rb and Al measured by both scanning XRF and ICP-MS in Core SPR0901-04BC agree with each other in general (Hendy et al., 2015), indicating that the XRF results of these elements reflect variations of the total elemental concentration. The variations of scanning XRF K, Rb, Ti, Mn and Si in Core SBB-8-2012 are very similar each other (Si is plotted in **Figure 5**). Aluminum content in our core is very low (the maximum intensity is less than 50 cps), so it is excluded in the discussion. Therefore, we compare Fe, K, Rb, Ti and Si contents in Core SBB-8-2012 with the PC1 and Fe in Core SPR0901-04BC.

Figure 3 shows the comparison of the two cores. Only two major similarities are certainly identified: (1) variations of K, Rb and Ti in the upper 12 cm (0-12 cm) of SBB-8-2012 are similar to the variations of PC1 during 1969-2008 in SPR0901-04BC; and (2) the high K, Rb and Ti contents below 36 cm depth in SBB-8-2012 are similar to the PC1 XRF elements in the massive olive layer during 1812-1840 in SPR0901-04BC. As we mentioned before, the sediment was broken at 12.5 cm depth during the transportation from USC to NTU, perhaps due to the sudden change in the sedimentary feature at this depth. The flood event of 1969 had been recorded in the sedimentary deposits of SBB (Schimmelmann et al., 2013). According to the report of Santa Barbara County Flood Control & Water Conservation District (https://www.countyofsb.org/uploadedFiles/pwd/Content/Water/1969FloodRpt.pdf), severe flood events occurred in 1964, 1967 and 1969, but "the 1969 12-hour rainfall equaled or exceeded the so-called 100-year storm in the upper Santa Ynez watershed". In addition, the Santa Barbara oil spill occurred in January and February 1969, which is the third-largest oil spill in the world (Foster et al., 1971). The severe oil spill in the Santa Barbara Channel could have affected sedimentation. Thus, possibly the 12.5-cm depth break may reflect the 1969 flood event and oil spill. If we use 2011 CE for the core top and 1969 CE for 12.5-cm depth, an estimated mean sedimentation rate can be calculated: 12cm/(2011-1969) = 0.29 cm/yr, which is slightly higher than the 0.22-0.26 cm/yr estimated by the ^{210}Pb dating. According to **Figure 3**, the PC1 XRF elements in SPR0901-04BC during 1770-1810 were very low. A strong drop in the PC1 XRF elements from 1815 to 1805 does not appear in the K, Rb and Ti in SBB-8-2012. If we assume the bottom of SBB-8-2012 is 1815 CE, then a mean sedimentation rate can be calculated: (51-12)/(1969-1815) = 0.25 cm/yr, which agrees with the 0.22-0.26 cm/yr estimated by the ^{210}Pb dating. We did not find gray layers identified in SPR0901-04BC. Although K, Rb and Ti contents in Core SBB-8-2012 show a peak value around 30 cm depth, this peak is not very outstanding and does not exist in Fe content. Thus, the above-mentioned age marks: (A) the 1969 flood event and oil spill at the 12-cm depth break and (B) 1815 CE at the bottom of Core SBB-8-2012 help us to further constrain the chronology. With the lamination and the ^{210}Pb dating estimations, we use a 0.29 cm/yr sedimentation rate for 0-12 cm and 0.25 cm/yr for 12-51 cm for constructing the chronology of the core. According to Inman and Jenkins (1999), the suspended sedimentary flux to SBB during the wet 25 years of 1969-1995 was five times greater than the previous 25 dry years (Schimmelmann et al., 2013). It is reasonable that the sedimentation rate in Zone III was higher. Nevertheless, based on the two sedimentation rates we calculate the chronology of the core which shows on the right-hand side of **Figure 2C**. The core contains a depositional history from 1815 CE to 2011 CE. We admit that the chronology assumes linear sedimentation rates in the segments and contains about 5% relative uncertainty. The chronology has an error of 1-2 years for the upper 12 cm deposition, and an error of 2-5 years between 12 cm and 51 cm depths.

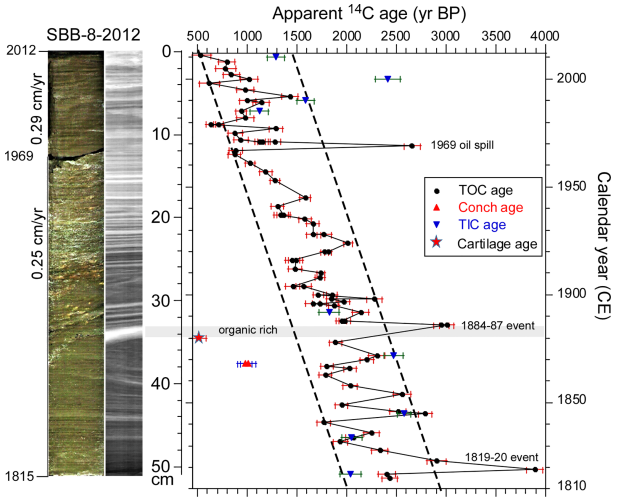

FIGURE 4 | The measured ^{14}C ages of all samples in Core SBB-8-2012. The two parallel dashed lines indicate the envelope of general variations of the measured ^{14}C ages on total organic carbon in the sediments except for three outstanding horizons.

3.3 ^{14}C Age and D$^{14}C_{TOC}$ Variation of the Core

Table 2 lists 89 AMS ^{14}C dates. Amongst these dates, 77 dates are for TOC and 12 dates are for TIC. These ^{14}C ages range from 516±71 to 3889±85 yr BP, much older than the depositional ages of 1815-2011 CE. Of the 77 TOC dates, one is animal cartilage and 13 dates are duplicated measurements on the sediments from 13 horizon samples. The duplicated measurements illustrate that the results are in good agreement within uncertainties, indicating the dating results are reliable. In the 12 TIC dates, 6 TIC dates are coupled with TOC dates from the sediments. They are generally in the same order of their coupled $^{14}C_{TOC}$ dates, reflecting approximately similar sources of TOC and TIC in the sediments. Two $^{14}C_{TIC}$ dates are from the same conch shell sample, showing agreement within uncertainties (**Table 2**). Four $^{14}C_{TIC}$ dates (marked with @ symbol in **Table 2**) are from independent layers, showing the ^{14}C ages ranging from 888±66 to 2577±71 yr BP. In this study, we will focus on the discussion of $^{14}C_{TOC}$ dates. Therefore, the $^{14}C_{TOC}$ dates from 62 horizons from the core will be used for interpretations of changes in paleoclimate and paleoceanography and the input of different sources of TOC to SBB.

Figure 4 displays the variations of apparent ^{14}C ages throughout the core. The age of the cartilage is the youngest, being 516±71 yr BP without reservoir age correction. However, the true age of this animal remain should be around 1880 CE based on the ^{210}Pb dating and varve counting. This means that if the organism formed in the water column in SBB, the basin water should have a ^{14}C reservoir age of at least 400 years which is much older than the reservoir age (233±60 years) of modern surface water in SBB (Ingram and Southon, 1996). The age of the conch shell is about 980~1010 yr BP, reflecting again the reservoir effect in the Santa Barbara Basin. These two ages imply that the reservoir age in SBB

may vary largely on annual-to-decadal time scales. It is interesting that the $^{14}C_{TOC}$ ages varied generally within the two paralleled dashed lines shown in **Figure 4** except for the three layers which have much older ages. The dashed line on the younger side covers the ages from 2000 yr BP at the bottom of the core to 500 yr BP on the core top. As the depositional age of the total core is 200 years, radioactive decay could not cause such a change. If the TOC of the samples on the younger side of the dashed line reflects primarily the organic matters mixed from terrestrial input (allogenic/allochthonous) and from endogenic input (autochthonous) through photosynthesis in the water column of SBB, then the significant age change (~1500 years) implies that either the reservoir age of the SBB water varied a lot during the past 200 years, or the ratio of allochthonous/autochthonous OC input has changed significantly and systematically. Nevertheless, the variations of the ^{14}C ages shown in **Figure 4** demonstrate that radiocarbon dating on either organic or inorganic carbon formed in the water column of SBB is problematic. Only terrestrial plant remains in the sediments appear as a valid way to provide "true" depositional ages in SBB.

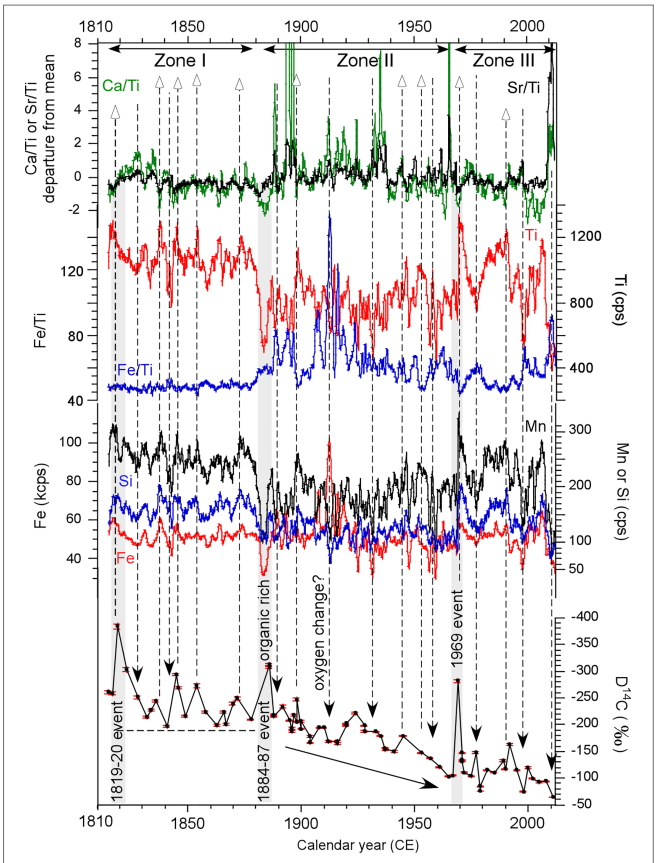

FIGURE 5 | Comparison of the variations in $D^{14}C_{TOC}$ values and the scanning XRF elemental contents in Core SBB-8-2012. In general, more depleted $D^{14}C$ value corresponds to higher siliciclastic elements (K, Ti, Si, Mn and Rb) and lower biogenic proxies (Ca/Ti, Sr/Ti and Fe/Ti); and vice versa. The dashed vertical lines with open arrow refer the periods of more depleted $D^{14}C$ value, whereas the dashed vertical lines with solid arrow show the intervals with less depleted $D^{14}C$ value.

Since the ^{14}C ages do not provide age meaning and our discussions focus on the ^{14}C variation of TOC, we use $D^{14}C_{TOC}$ values for further discussion.

3.4 Elemental Contents Measured by Scanning XRF

As the fore-mentioned scanning XRF elements represent total contents of all phases including organic, authigenic and detrital components. The elements which have meaningful results (by meeting the two criteria) show the intensity in the following order with their average intensity (cps) in the bracket: Fe (51206) > Ca (4771) > Sr (2399) > Cl (1241) > K (1015) > Ti (919) > Rb (597) > Zn (352) > Zr (235) > Mn (213) > Ni (205) > Y (192) > Cu (144) > Si (138) > S (82) > Pb (50). In this study, we only select Fe, Ca, Sr, K, Rb, Ti, Si and Mn for discussion.

The K, Ti, Rb, Si and Mn are lithophile elements that mainly come from terrestrial detrital input (Goldschmidt, 1926). However, Si and Mn can also be influenced by diagenesis and biogenic input. **Figures 3**, **5** show the variations of K, Ti, Rb, Si and Mn are positively correlated, indicating that they likely have the same sources. The correlation coefficient (R^2) between K and Ti, Si, Mn, or Rb are 0.96, 0.84, 0.91 and 0.74, respectively, implying that the scanning XRF Si and Mn were mainly from detrital input. These elements were considered as siliciclastic elements and grouped in PC1 by Hendy et al. (2015). Since Ti is commonly attributed to terrigenous inputs in pelagic sediments, we can use it to normalize for siliciclastic input. The lithophile elements (K, Ti, Si and Mn) appear different average contents: high in Zone I, low in Zone II and moderately high in Zone III. For example, the average intensities (cps) with standard deviation (numbers of data points) of K content are 1190±120 (n = 755), 867±136 (n = 1019) and 1044±208 (n = 633) in Zone I (1815-1880 CE), II (1880-1969 CE) and III (1969-2011 CE), respectively. Similarly, the average intensities of Ti content are 1071±109, 789±139 and 947±212 in Zone I, II and III, respectively. The changes in the average contents of the lithophile elements in three zones indicate that the terrestrial detrital input to the sediments was the highest in Zone I and the lowest in Zone II, which helps us in understanding of the $D^{14}C_{TOC}$ change of the core.

Although Fe, Ca and Sr are also lithophile elements, but their contents in the sediments can be influenced by the chemical and biological conditions in the water column. These elements can have significantly authigenic compositions compared with the detrital compositions. For example, Ca and Sr are easy to co-precipitate into carbonates, resulting a strong positive correlation between the two. However, the scanning XRF Ca and Sr do not have a strong correlation (R^2 = 0.4), although the variations of the two are very similar (**Figures 5**, **6**). As mentioned before, oxidation (e.g., $FeS_2 + O_2 \rightarrow Fe_2O_3 + H_2S$) of the scanned surface sediment layer when the core opened to the air for long time could affect some scanning XRF elements including Fe, Ca and Sr. Interpretations of the XRF Fe, Ca and Sr results should be caution. The Ca/Ti and Sr/Ti are considered as indicators of biogenic components to be normalized for the siliciclastic input (Hendy et al., 2015). Their variations are dominated by the variations of Ca

and Sr intensities. The higher Ca/Ti and Sr/Ti reflect a stronger productivity.

The variations of Ca/Ti and Sr/Ti shown in **Figure 5** vary generally opposite to the siliciclastic elements (K, Ti, Si and Mn), indicating a higher portion of biogenic component corresponding to the lower siliciclastic component. It is interesting to see that less depleted (or less negative) $D^{14}C$ values correspond to higher Ca/Ti and Sr/Ti values; and vice versa (**Figure 5**). This means that more OC formed in the water column and less old carbon from siliciclastic source lead to smaller ^{14}C reservoir age. In general, Ca/Ti and Sr/Ti values were high in Zone II, especially several high Ca/Ti peaks, reflecting strongly increased biogenic input into the sediments. These changes should reflect variations in the chemical and oceanographic conditions in SBB.

Although Hendy et al. (2015) considered Fe as a siliciclastic element and used Fe/Ti as a proxy of terrigenous input, Fe can be strongly affected by redox conditions in the environment. The Fe profile in **Figures 3, 5** shows that the highest content throughout the core was around 1910 CE, whereas other scanning XRF elements were low. The high Fe content in this period is also visible in the core photo, showing the brown band. In **Figure 5**, Fe/Ti shows totally different patterns with the other siliciclastic elements: low and relatively invariant values in Zone I, high and strongly fluctuated values in Zone II, and moderately high and variant values in Zone III. The Fe/Ti values in Zones II and III clearly co-vary with Ca/Ti and Sr/Ti but opposite to the siliciclastic elements, reflecting biogenic input into the sediments. This situation is quite different from the Fe variations in Core SPR0901-04BC (Hendy et al., 2015). Nevertheless, we are not able to use Fe or Fe/Ti variations as an indicator of siliciclastic input given by Hendy et al. (2015). Instead, the Fe/Ti in Zones II and III together with probably Ca/Ti and Sr/Ti reflected biogenic input into the sediments. Another reason for the Fe profiles discrepancies between our core and Core SPR0901-04BC may be attributed to the oxidation effect of Core SBB-8-2012 as it opened to the air for many years. If it is true, the scanning XRF Fe/Ti and Ca/Ti do not represent the original situation in the sediments. To avoid the oxidation effect, we use Sr/Ti only as an indicator of biogenic input.

Another important phenomenon is that all XRF elements were the lowest in the light band at 34-cm depth (around 1885 CE). This light band showed a strongly depleted $D^{14}C_{TOC}$ value (**Figure 5**) with the lowest contents of all scanning XRF elements and less density, indicating that this layer may be enriched in organic matter. Although we do not know the cause of this organic rich layer, a few historic references may provide insight on this event. According to the timeline of Santa Barbara (https://www.santabarbaraca.gov/services/community/historic/historysb/timeline.asp), crude oil was first extracted from the Santa Barbara Channel along the coast at Summerland in 1886. Another unusual observation was that a large abundant kelp forest about 300 yards off Santa Barbara coast in 1887 (Fewkes, 1889), which occurred in other places along the coast of Southern California. Schimmelmann et al. (1995) interpreted this as evidence that no severely destructive storm and wave events has occurred in Santa Barbara for a few years prior to 1887 CE. Less terrestrial detrital input due to less surface runoff and highly abundant marine productivity caused by some oceanographic condition changes agree with our results. Whether there was a significant influence from the first extraction of crude oil in the Santa Barbara Channel is unclear. Nevertheless, the scanning XRF elemental contents will help us in understanding the paleoclimate and paleoceanography change on annual-to-multidecadal scales.

In summary, the siliciclastic elements (K, Ti) reflect mainly terrigenous input from the river inflow around SBB, whereas Ca/Ti, Sr/Ti and Fe/Ti reflect chiefly biogenic input from the marine system in SBB. The two groups have generally opposite trend, and higher values of the siliciclastic elements and lower values of biogenic indicators correspond to less depleted (larger) $D^{14}C_{TOC}$ values; and vice versa. In this study, (K+Ti)/2 is used for terrigenous input, whereas Sr/Ti is used for biogenic input. The sediments of Core SBB-8-2012 showed significant changes in terms of geochemical and biological features from Zone I to Zone II after an organic-rich layer was deposited around 1885

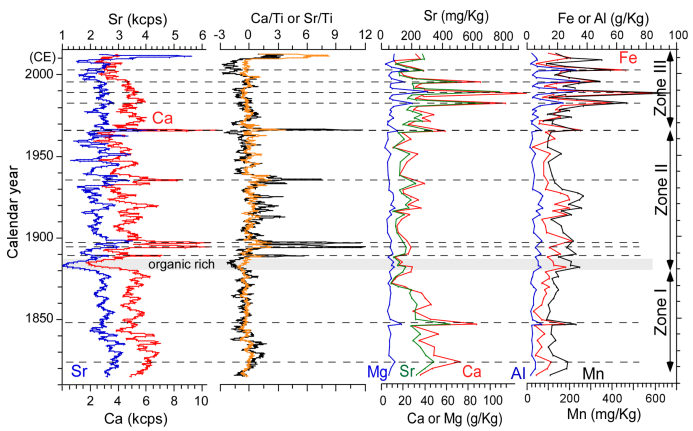

FIGURE 6 | Comparison of the variations in elemental contents measured by XRF scanning and ICP-OES methods in Core SBB-8-2012. Note that elemental concentration has different units, being g/Kg for Fe, Mg and Ca, and mg/Kg for Mn and Sr. The horizontal dashed lines show the comparisons when the acid-leachable elemental concentrations were relatively high.

CE (34-35 cm depth) with more terrigenous input in Zone I and more biogenic input in Zone II.

3.5 Acid-Leachable Elemental Concentrations Measured by ICP-OES

The ALE concentrations of Ca, Fe, Mg, Al, Sr and Mn were listed in **Table 3**. Their average concentrations (mg/Kg) with standard deviations are in the following order: Ca (34299±21926) > Fe (18655±13279) > Mg (9685±5738) > Al (6835±6753) > Sr (202±120) > Mn (180±94).

Figure 6 exhibits the ALE concentrations of Ca, Mg, Sr, Fe and Mn and comparisons with the scanning XRF results in the core. The ALE Ca and Sr have a strong correlation ($R^2 = 0.95$), indicating the same source inputs and similar chemical behavior between the two. The same feature does not occur between the scanning XRF Ca and Sr. This is because the ALE Ca and Sr come mainly from authigenic phase, whereas the scanning XRF Ca and Sr count for both authigenic and detrital phases. The correlations (R^2) between ALE Fe and ALE Mg, ALE Al or ALE Mn are 0.86, 0.85 and 0.83, respectively, showing that they come from the same sources. The ALE Fe, Mg, Al and Mn have no significant correlations with the ALE Ca ($R^2 < 0.5$) except for five high Ca points (>60 g/Kg), indicating that these five layers contain abundant elements from the authigenic input. In addition, Zone I had the lowest ALE Fe, Mg, Al and Mn, but moderately high ALE Ca and Sr. This means that the sediments in Zone I have more siliciclastic feature because detritus contain less ALE Fe, Mg, Al and Mn.

The comparisons of the scanning XRF contents and the ALE concentrations of Ca and Sr show significant discrepancies in terms on long and short time scales. The ALE concentrations of Ca and Sr were relatively low in Zone II, while the scanning XRF Ca and Sr did not show this. Secondly, several distinct ALE Ca and Sr peaks (i.e., around 1822, 1849, 1982, 1994 and 1999) were not corresponding either to scanning XRF Ca and Sr or Ca/Ti and Sr/Ti. As mentioned before, scanning XRF involves a measured element in all phases, with a matrix effect, very small scan area and semi-quantitative nature. It is understandable that the scanning XRF results may not have relationship with the ALE elements. However, the peaks of ALE elements should reflect oceanic conditions for higher productivity, while the troughs of ALE elements may correspond to low productivity periods. The variations of the ALE concentrations will shed the light on chemical and biological conditions in the water column of SBB.

4 DISCUSSIONS

4.1 Factors Influencing $D^{14}C$ Variation in Core SBB-8-2012

OC in the sediments of the SBB depo-center comes from three possible major sources: (1) biological products in the marine system of the Santa Barbara Channel (Thunell, 1998; Barron and Bukry 2010); (2) terrestrial inputs from surface runoff which comes mainly from the Ventura River, Santa Clara River and creeks in the Santa Ynez Mountain drainage basin (Kolpack and Drake, 1984; Thunell et al., 1995; Schimmelmann and Lange, 1996); and (3) fossil OC from leakages in the marine system (e.g., oil spill in surface water; gas and oil are seeping from oil seepage such as from the Coal Oil Point seep field) (Hornafius et al., 1999) and/or lateral transported sediments from other locations inside or outside of SBB (**Figure 7**).

The ^{14}C activity of the first OC source which is produced in the SBB water column is influenced by (1) the atmospheric ^{14}C variation and CO_2 exchange with the water; (2) variation of oceanic circulation in the SBB channel; and (3) fossil C emission from the seafloor. In general, the $D^{14}C$ of the atmospheric CO_2 is much greater than that of the fossil C emission which is -1000‰. The atmospheric $D^{14}C$ at 1950 CE was 0‰ and strongly increased due to nuclear tests (reached to 785‰ in North Hemisphere in 1964) (Hua et al., 2013). The nuclear bomb ^{14}C signal reached a peak during 1970~1976 in the ocean (Grottoli and Eakin, 2007). The highest $\Delta^{14}C$ value was ~140‰ in 1974 in the Atlantic coral (Druffel, 1996), and was ~190‰ in 1975 in the Pacific coral (Andrews et al., 2016), showing the bomb ^{14}C significantly affected the ^{14}C reservoir age in oceans.

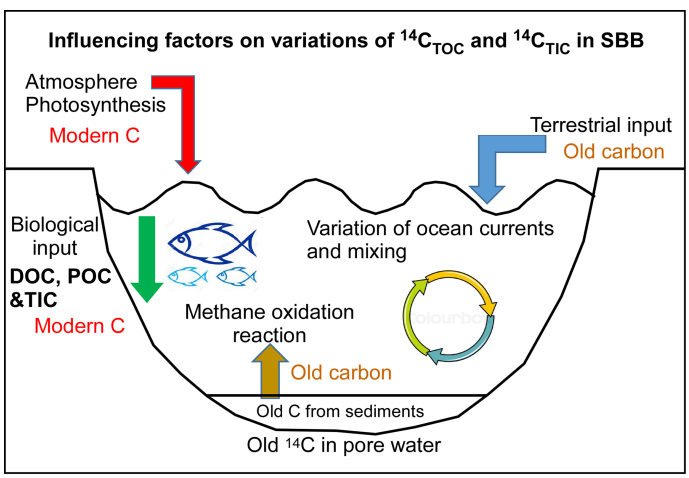

FIGURE 7 | A conceptual box model of the influencing factors on the carbon cycles in Santa Barbara Basin.

On the other hand, fossil carbon input in SBB is a well-known phenomenon. The Coal Oil Point seep field located at near shore of SBB is one of the largest natural submarine hydrocarbon emission areas in the world (Allen and Mikolaj, 1970; Valentine et al., 2010). Methane and crude oil are emitted from the seafloor (Hornafius et al., 1999). Most of the emitted hydrocarbons are consumed by methanotrophic bacteria in surface sediments or in the water column (Treude and Ziebis, 2010). The fossil carbon emission from the seafloor in SBB may vary with tidal changes and/or seismic activity (Hornafius et al., 1999; Eichhubl et al., 2000; Boles and Clark, 2001).

According to Kennett et al. (1997), the oceanic circulation in the Santa Barbara Channel influences ^{14}C activity of the marine reservoir as follows: The ^{14}C-depleted California current and associated southern California Eddy flow southward, and bring cold and low salinity water dominated in the winter-spring season (**Figure 1**). In contrast, the California counter-current flows northward and transports the relatively ^{14}C-rich, warm and saline equatorial water along the southern California coast during the summer-fall season (**Figure 1**). This annual circulation pattern and upwelling of Pacific intermediate water along the California coast can be modified by summer insolation change (Bakun, 1990; van Geen and Husby, 1996), and ENSO events (McGowan, 1984; Rassmusson, 1984; Ramage, 1986) on interannual scales.

Although many previous studies have found the anomalies of marine ^{14}C reservoir age in SBB (e.g., Ingram and Kennett, 1995; Kennett and Ingram, 1995; Kennett et al., 1997; Roark et al., 2003; Schimmelmann et al., 2006; Hendy et al., 2013; Du et al., 2018), those studies are generally for long time scales (>1000 years). Below, we will discuss the variations of $D^{14}C_{TOC}$ and their causes during 1815~2011 CE. We will focus our discussion on ENSO influences.

4.2 Causes of Strong Depleted $D^{14}C$ Excursions in Core SBB-8-2012

In **Figures 4**, **5**, the three negative $D^{14}C_{TOC}$ (old age) excursions around 1964-69, 1884-87 and 1819-20 CE could be attributed to "extra old carbon influence". The $D^{14}C_{TOC}$ values of these excursions exceeded significantly the general variation envelope (two paralleled dash lines), so that their old carbon influence should be caused by some abnormal reasons. For the youngest excursion, one reason could be the oil spill event in 1969. During a 10-day period in early 1969, about 4 million gallons of crude oil spilled into the Santa Barbara Channel after a blowout six miles offshore on a Union Oil drilling platform (Foster et al., 1971). This disaster is the third largest oil spill in the world up to date. Organisms and particles could take up the oil to deposit on the seafloor, so that the $D^{14}C_{TOC}$ of this layer could be strongly influenced by the oil. In addition, as we discussed above, flood events in 1964, 1967 and 1969 (especially the 1969 flood) could transport larger portion of old OC in terrigenous sediments in the TOC of this layer. Soil OC from terrestrial input may have ^{14}C age of several thousand years or older than the date of their erosion and deposition. Thus, strong flood events may carry those soil OC into the SBB sediments. The peaks of the lithophile elements in the same layer shown in **Figure 5** support the flood impact.

For the 1884-87 excursion, the strongly depleted $D^{14}C_{TOC}$ occurred on the layer of organic rich and minimum concentrations of all scanning XRF elements (**Figure 5**). The low scanning XRF elements reflect that the depleted $D^{14}C_{TOC}$ should not be attributed to flood events. Two possible events may explain the old carbon influence: 1. Possible sudden short leak of fossil carbon from the Coal Oil Point seep field during the first extraction in 1886; and 2. Strongly increased upwelling from the Pacific deep water entered the basin, which might bring abundant nutrients to cause a surge of biological productivity in SBB, reflected by a large abundant kelp forest along Santa Barbara coast in 1887 (Fewkes, 1889). The ^{14}C activity in the Pacific deep water should be much lower than that of surface water. The abundant OC deposited in the sediments can be preserved due to anoxic conditions on the seafloor of SBB. The above hypothesis needs more direct evidence to support it, especially the reconstruction of upwelling strength during this period. Analysis of the organic compounds in this layer would help reveal its source.

The 1819-20 excursion in the $D^{14}C_{TOC}$ may be explained by the strong input of soil OC into the SBB sediments as the scanning XRF Si, Ti and K (detrital origins) showed high contents in this layer (**Figures 5**, **9**). In addition, if the 1812 Ventura earthquake (also known as the Santa Barbara earthquake) (7.1–7.5 magnitude) caused strongly increased fossil carbon leakage from the Coal Oil Point seep field (Eichhubl et al., 2000), then the leaked fossil carbon could be consumed by methanotrophic bacteria and deposited in the sediments in this layer, given the chronology has an uncertainty of several years in this part.

4.3 The $D^{14}C_{TOC}$ Changes in Different Zones

The $D^{14}C_{TOC}$ variation shown in **Figure 5** has experienced three different features. If the $D^{14}C_{TOC}$ value at 35-35.2 cm is excluded as this sample is unlike some sediment samples (organic rich), the mean $D^{14}C_{TOC}$ values and their standard deviations for Zone I, II and III are -247.0±44.4‰ (n = 22), -181.9±34.1‰ (n = 34) and -119.7±45.2‰ (n = 21), respectively. Since the core sediments have only about 200-year history, ^{14}C decay (half-life is 5730 years) should not cause such a large difference. In Zone I (1815~1880 CE), the maxima $D^{14}C_{TOC}$ values (ca. youngest ages) are around -201.8‰ (-197.5‰ at 44.6 cm, -199.4‰ at 39.2 cm, -200.9‰ at 38.1 cm and -209.4‰ at 35.5 cm), no apparent enrichment trend (referred by a horizontal dash line in **Figure 5**). The much smaller (lower, or lighter) average $D^{14}C_{TOC}$ value and relatively constant maximum $D^{14}C_{TOC}$ value of Zone I indicate that the OC in the sediments during this period contains more old carbon influence and the carbon reservoir effect of the marine system may be larger. The scanning XRF K, Ti, Si and Mn were higher in Zone I, which provides evidence of more soil OC from terrigenous sediments (**Figure 5**). Other two contributions to the lower mean $D^{14}C_{TOC}$ value in Zone I could be: (1) higher emission flux of fossil carbon from the Coal Oil Point seep field compared to the later periods since the extraction of the fossil fuel began in 1886; and (2) lower marine productivity compared

to the later periods. The second hypothesis can be seen in low values of Ca/Ti, Sr/Ti and Fe/Ti which are indicators of biogenic components in the sediments. For the first hypothesis, more studies on the OC budget in SBB are needed.

In Zone II (1885-1969 CE), the $D^{14}C_{TOC}$ value has smaller variations and show an apparently increasing trend. The $D^{14}C_{TOC}$ enrichment trend in Zone II can be explained by two reasons: one is that the fossil carbon emission from the seafloor had been reduced since the extraction beginning in 1886; and another one is increased the biogenic carbon flux into the sediments perhaps due to an enhanced nutrient availability in SBB. As the nutrient supply increased, the primary productivity in SBB produced more OC from endogenic input in the water column. Thus, the portion of OC from terrigenous sediments became smaller. In fact, scanning XRF had relatively lower contents in Zone II, reflecting less contribution of terrigenous sediments. High Ca/Ti, Sr/Ti and Fe/Ti values in Zone II illustrate high biogenic components in the sediments.

The $D^{14}C_{TOC}$ values in Zone III (1969~2011 CE) still show a slightly enrichment trend, and the three maxima values are -75.8‰ in 1977, -74.0‰ in 1998 and -64.3‰ in 2011. Since the nuclear bomb ^{14}C signal from the atmospheric CO_2 entered into the ocean in late 1960s and reached its peak in 1975, the enrichment trend of the $D^{14}C_{TOC}$ in Zone III can be influenced by the bomb ^{14}C. However, none of the $D^{14}C_{TOC}$ values are greater than zero in the core (**Table 2**), indicating that the bomb ^{14}C signal is masked by the ^{14}C reservoir effects in SBB and older terrestrial OC input.

If we assume the cartilage sample at 36 cm depth was formed in the water column, this sample does not contain OC from terrigenous sediments, and has a $D^{14}C$ value of -62.2‰ and ^{14}C age of 516±71 yr BP (**Table 2**). The calibrated ^{14}C age without reservoir correction of this sample is 92.5% in the range of 454-660 yr BP (2σ) or 560±105 yr BP by using the calibration curve IntCal13. This age is significantly older than the ^{14}C reservoir age (233±60 yr) of modern ocean surface water in SBB (Ingram and Southon, 1996). If we use the $D^{14}C$ value of this sample as the endmember of marine biological carbon in SBB, we may estimate the OC contribution from the marine system and terrigenous input. In **Figure 5**, the heavier (higher) $D^{14}C$ values are generally corresponding to low scanning XRF K, Ti, Si and Mn (siliciclastic), and high Ca/Ti, Sr/Ti and Fe/Ti (biogenic), whereas the lighter (lower) $D^{14}C$ value are generally corresponding to high siliciclastic elements but low biogenic elements except for the organic-rich layer around 1885 CE.

4.4 ENSO Influence on the $D^{14}C$ Variation of Core SBB-8-2012

The variations of the $D^{14}C_{TOC}$ in the sediments show interannual-to-decadal cycles (**Figure 5**), reflecting the impact of climatic changes on the terrigenous input of soil TOC and on the productivity of biological marine TOC. Since the precipitation in southern California including Santa Barbara is strongly influenced by ENSO (McGowan, 1984) and oceanic circulation in Santa Barbara Channel is also related to ENSO (Rassmusson, 1984), the $D^{14}C_{TOC}$ variation may be affected by ENSO. For this purpose, we have done spectrum analysis on both the Southern Oscillation Index (SOI) and the $D^{14}C_{TOC}$ record. **Figure 8** displays the results. The monthly data of SOI from 1866 to 2021 was downloaded from https://crudata.uea.ac.uk/cru/data/soi/ (Ropelewski and Jones, 1987; Allan et al., 1991). The cycles of 3.6-yr, 5.7-yr and 6.4-yr fall into the 4-7 year band of El Niño/La Niña cycles. The $D^{14}C$ data sets have age intervals on the order of 1-8 years (**Table 2**). In order to perform the spectrum analysis, the interval should be uniform. Thus, we interpolate the data to annual resolution by using the excel program (linear interpolation), and the spectrum analysis shows that the $D^{14}C_{TOC}$ record has cycles of 4.9-yr, 5.8-yr, 7.3-yr, 8.7-yr, 9.7-yr and 13-yr (**Figure 8B**). As the resolution of $D^{14}C$ data allows the highest frequent cycle of 6-yr, the 4.9-yr cycle is not considered. The group of 5.8-yr

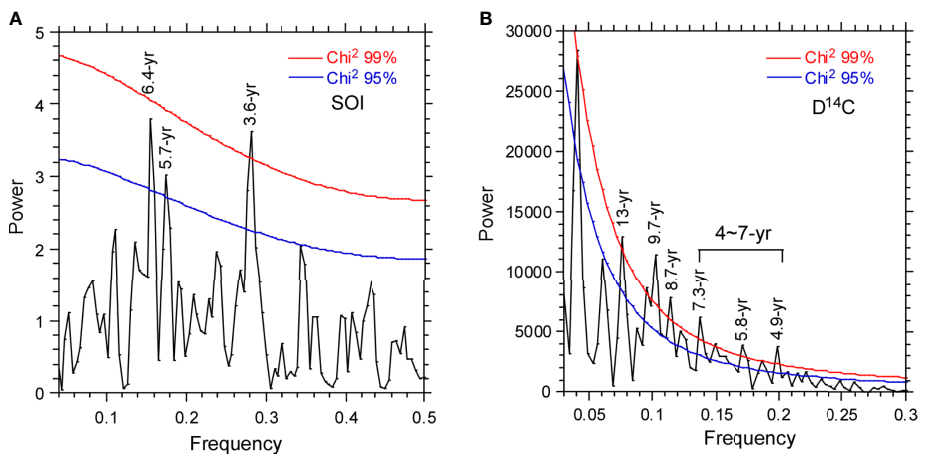

FIGURE 8 | Spectrum analysis for the SOI (data source: https://crudata.uea.ac.uk/cru/data/soi/) **(A)** and the D14CT OC **(B)**. The blue curve and red curve indicate confidence level and 95% and 99%, respectively. The numbers marked in the plots denote the possible cycles above 95% confidence level.

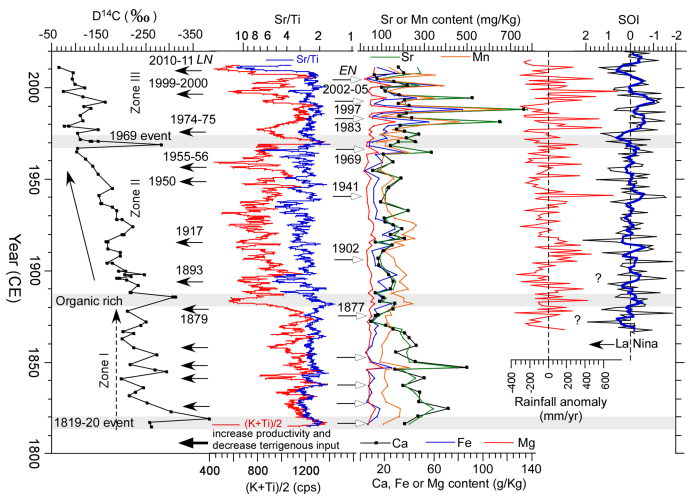

FIGURE 9 | Comparisons of the $D^{14}C$, scanning XRF elemental content, ICP-OES measured acid-leachable elemental concentration with the historical rainfall (the data was downloaded from **https://www.santabarbaraca.gov/SBdocuments/Advisory_Groups/Water_Commission** before it was removed.) and SOI records. The open head arrows refer El Niño events, and the solid head arrows reflect La Niña events. Note that the relationship between the rainfall in southern California and ENSO events is not fixed. For example, negative SOI values around late 1890s (shown by a question mark there) did not result in high rainfalls. Another question mark around 1870 shows the comparison is not valid, because low rainfall during this La Niña event would lead to high ALE contents but low scanning XRF siliciclastic elemental contents. This outliner may be caused by chronological uncertainty.

and 7.3-yr cyclicities may reflect the 4~7-year ENSO cycle, whereas the group of 8.7-yr, 9.7-yr and 13-yr cyclicities may represent double of the 4~7-year ENSO cycle.

Since the $D^{14}C_{TOC}$ record has only ~200 years, changes in summer insolation may vary small. Therefore, we focus on the influence of ENSO on the rainfall and oceanic circulation variations in SBB. During El Niño year, the marine biological productivity should decrease (Lange et al., 1987), and heavy rains are frequent along southern California. The ratio of terrigenous soil OC/biogenic OC increases with high input of siliciclastic elements and low ALE in the SBB sediments during El Niño events. In contrast, during La Niña years stronger California Current and upwelling bring abundant nutrients to elevate the marine productivity, resulting higher biological OC content in the sediments and higher $D^{14}C_{TOC}$.

In **Figure 9**, we compare the $D^{14}C_{TOC}$, scanning XRF siliciclastic elements (K+Ti)/2, proxy of biogenic components (Sr/Ti) and ALE contents (Ca, Fe, Mg, Sr and Mn) with the SOI and south coast annual precipitation records. The comparisons show that during strong El Niño years (open head arrows, e.g., 1902, 1941, 1969, 1982-83, 1997 and 2002-05) higher (K+Ti)/2, lower Sr/Ti, minima the ALE contents and decreased $D^{14}C_{TOC}$ were dominant. In contrast, low scanning XRF (K+Ti)/2, higher Sr/Ti, high ALE contents and enriched $D^{14}C_{TOC}$ were corresponding La Niña conditions (solid head arrows). It is worth to mention that our record cannot be accurate on annual scale, so that comparison with low rainfall periods is more reasonable than with individual El Niño or La Niña years. The above comparison between our record with the instrumental records (rainfall and SOI) perhaps also demonstrates that our chronology of the core is reliable as the instrumental records have precise age control.

5 CONCLUSIONS

A 51-cm long core SBB-8-2012 from SSB was dated by ^{210}Pb and varve counting. The chronology of the core was refined by comparing with a previous well-dated core from the same area, showing the depositional history of 1815-2011 CE with sedimentation rates of 0.25-0.29 cm/yr. The core has been measured for scanning XRF on an ITRAX core scanner, acid-leachable (0.5N HCl) elemental concentrations by an ICP-OES, and a total of 89 ^{14}C dates by AMS. Based on the sedimentary features and the above measured results, the core sediments can be classified into three zones: Zone I (1815-1880 CE) contains denser sediments with thinner laminations, higher scanning XRF K, Ti, Si, Mn and Rb, lower Fe/Ti, Ca/Ti and Sr/Ti, and lower $D^{14}C_{TOC}$ values. Zone II (1880-1969 CE) includes less dense sediments with thicker laminations, the lowest scanning XRF K, Ti, Si, Mn and Rb, highest Fe/Ti, Ca/Ti and Sr/Ti, and strongly enriched $D^{14}C_{TOC}$ trends. Zone III (1969-2011 CE) covers well laminated sediments with high $CaCO_3$ contents, high acid-leachable elemental concentrations, strongly fluctuated XRF elemental contents and higher $D^{14}C_{TOC}$ values.

The apparent ^{14}C ages of the 200-year sediment core vary between 500 and 4000 yr BP with $D^{14}C$ values ranging from -62.2‰ to -383.8‰, reflecting influences of terrigenous soil OC input, fossil carbon emission from the Coal Oil Point seep field and ^{14}C reservoir effect controlled by oceanic and atmospheric circulations. The three strongly negative $D^{14}C_{TOC}$ excursions around 1819-20, 1884-87 and 1964-69 CE might be respectively related to the 1812 Santa Barbara earthquake, the first oil extraction in 1886 and unusual marine biological productivity in 1887, and the 1969 oil spill as well as flood

events. The long-term mean $D^{14}C_{TOC}$ shifts in three zones were probably caused by relatively high terrigenous soil OC input and fossil carbon emission from the Coal Oil Point seep field in Zone I, reduced fossil carbon emission due to the oil extraction and enhanced biological productivity in Zone II, and nuclear bomb ^{14}C influence in Zone III. Nevertheless, the ^{14}C reservoir effect in Santa Barbara Channel has been changed significantly during the past 200 years.

The ENSO events show strong influences on the $D^{14}C_{TOC}$, detrital elemental content and acid-leachable elemental concentration in the SBB sediments. During the La Niña period, stronger upwelling and northerly California Current bring nutrient enriched water into SBB and lead to higher productivity. Combining the effect of less terrigenous soil OC input during the La Niña period, lower scanning XRF K, Ti, Si, Mn and Rb, higher acid-leachable elements and higher $D^{14}C_{TOC}$ values can be resulted in the sediments. During the El Nino period, the phenomena are opposite.

AUTHOR CONTRIBUTIONS

H-CL supervised the study, performed sampling of the core, participated lab experiment and wrote the manuscript. YC conducted the study for his MSc thesis. WB provided the core, initiated and discussed the study. MZ discussed the study and helped in revising the manuscript. SM and T-TS helped in data process. All authors contributed to the article and approved the submitted version.

DATA AVAILABILITY STATEMENT

Publicly available datasets were analyzed in this study. This data can be found here: SOI (data source: https://crudata.uea.ac.uk/cru/data/soi/).

FUNDING

This study was supported by grants from Ministry of Science and Technology of Taiwan (MOST 106-2116-M-002-012, MOST 107-2116-M-002-005, MOST 108-2116-M-002-012 and MOST 109-2116-M-002-018) to H-CL, and by the National Natural Science Foundation of China (Grant No. 41630966) to MZ.

ACKNOWLEDGMENTS

We thank Ms. Su-Chen Kang and Ms. Chun-Yen Chou at the NTUAMS Lab for their help in the AMS ^{14}C dating. The iTRAX Lab in the Department of Geosciences and the NTUAMS Lab in the Instrumentation Center at NTU are acknowledged for their contribution to this study.

SUPPLEMENTARY MATERIAL

The Supplementary Material for this article can be found online at: https://www.frontiersin.org/articles/10.3389/fmars.2022.823793/full#supplementary-material

REFERENCES

Allan, R. J., Nicholls, N., Jones, P. D. and Butterworth, I. J. (1991). A Further Extension of the Tahiti-Darwin SOI, Early SOI Results and Darwin Pressure. *J. Climate* 4, 743–749. doi: 10.1175/1520-0442(1991)004<0743:AFEOTT>2.0.CO;2

Allen, A. A. and Mikolaj, P. G. (1970). Natural Oil Seepage at Coal Oil Point, Santa Barbara, California. *Science* 170, 974–980. doi: 10.1126/science.170.3961.974

Andrew, S. and Peter, A. C. (1977). Sedimentation and Climatic Patterns in the Santa Barbara Basin During the 19th and 20th Centuries. *Geolog. Soc. America Bull.*, 88, (8). 1161–1172. doi: 10.1130/0016-7606(1977)88<1161:SACPIT>2.0.CO;2

Andrews, A. H., Asami, R., Iryu, Y., Kobayashi, D. R. and Camacho, F. (2016). Bomb-Produced Radiocarbon in the Western Tropical Pacific Ocean: Guam Coral Reveals Operation-Specific Signals From the Pacific Proving Grounds, *J. Geophys. Res. Oceans* 121, 6351–6366. doi: 10.1002/2016JC012043

Bakun, A. (1990). Global Climate Change and Intensification of Coastal Ocean Upwelling. *Science* 247, 198–201. doi: 10.1126/science.247.4939.198

Barron, J. A. and Bukry, D. (2010). Santa Barbara Basin Diatom and Silicoflagellate Response to Global Climate Anomalies During the Past 2200 Years. *Quaternary Int.*, 215, 34–44. doi: 10.1016/j.quaint.2008.08.007

Barron, J. A., Bukry, D. and Hendy, I. L. (2015). High-Resolution Paleoclimatology of the Santa Barbara Basin During the Medieval Climate Anomaly and Early Little Ice Age Based on Diatom and Silicoflagellate Assemblages in Kasten Core SPR0901-02kc. *Quat. Int.* 387, 13–22. doi: 10.1016/j.quaint.2014.04.020

Baskaran, M. and Krishnamurthy, R. V. (1993). Speleothems as Proxy for the Carbon Isotope Composition of Atmospheric CO2. *Geophys. Res. Lett.* 20 (24), 2905–2908. doi: 10.1029/93GL02690

Baskaran, M. and Iliffe, T.M. (1993). Age Determination of Recent Cave Deposits Using Excess 210Pb—a New Technique. *Geophys. Res. Lett.* 20, 603–606.

Berelson, W. M., Morine, L., Sessions, A., Rollins, N., Fleming, J. C. and Schwalbach, J. (2019). Santa Barbara Basin Flood Layers: Impact on Sediment Diagenesis. In: From the Mountains to the Abyss: The California Borderland as an Archive of Southern California Geologic Evolution. *SEPM Special Publ. No. 110* p, 233–240. doi: 10.2110/sepmsp.110.11

Bograd, S. J. and Lynn, R. J. (2001). Physical-Biological Coupling in the California Current During the 1997–99 El Niño-La Niña Cycle. *Geophys. Res. Lett.* 28 (2), 275–278. doi: 10.1029/2000GL012047

Bograd, S. J., Schwing, F. B., Castro, C. G. and Timothy, D. A. (2002). Bottom Water Renewal in the Santa Barbara Basin. *J. Geophys. Res.* 107 (C12). 3216. doi: 10.1029/2001jc001291

Boles, J. R. and Clark, J. F. (2001). Temporal Variation in Natural Methane Seep Rate Due to Tides, Coal Oil Point Area, California. *J. Geophys. Res.* 106, 27077–27086. doi: 10.1029/2000JC000774

Bray, N. A., Keyes, A. and Morawitz, W. M. (1999). The California Current System in the Southern California Bight and the Santa Barbara Channel. *J. Geophys. Res.* 104 (C4), 7695–7714. doi: 10.1029/1998jc900038

Browne, D. R. (1994). Understanding the Oceanic Circulation in and Around the Santa Barbara Channel. *Fourth California Islands Symposium: Update Status Resour.* (Santa Barbara Museum of Natural History: Santa Barbara, California), 27–, 34.

Davis, C. V., Ontiveros-Cuadras, J. F., Benitez-Nelson, C., Schmittner, A., Tappa, E. J., Osborne, E., et al. (2019). Ongoing Increase in Eastern Tropical North Pacific Denitrification as Interpreted Through the Santa Barbara Basin Sedimentary $\delta^{15}n$ Record. *Paleoceanogr. Paleoclimatol.* 34, 1554–1567. doi: 10.1029/2019PA003578

Druffel, E. M. (1996). Post-Bomb Radiocarbon Records of Surface Corals Tropical Atlantic Ocean. *Radiocarbon* 38, 563–572. doi: 10.1017/S0033822200030095

Du, X. J., Hendy, I. and Schimmelmann, A. (2018). A 9000-Year Flood History for Southern California: A Revised Stratigraphy of Varved Sediments in Santa Barbara Basin. *Mar. Geol.* 397, 29–42. doi: 10.1016/j.margeo.2017.11.014

Emmer, E. and Thunell, R. C. (2000). Nitrogen Isotope Variations in Santa Barbara Basin Sediments: Implications for Denitrification in the Eastern Tropical North Pacific During the Last 50,000 Years. *Paleoceanography* 15 (4), 377–387. doi: 10.1029/1999pa000417

Eichhubl, P., Greene, H. G., Naehr, T., Maher, N. (2000). Structural Control of Fluid Flow: Offshore Fluid Seepage in the Santa Barbara Basin, California. *Geochem. Explor.* 69–70, 545-549. doi.org/10.1016/S0375-6742(00)00107-2

Fewkes, J. W. (1889). Across the Santa Barbara Channel. *Am. Nat.* 23, 211–217 387-394. doi: 10.1086/274906

Foster, M., Charters, A. C. and Neushul, M. (1971). The Santa Barbara Oil Spill. Part 1: Initial Quantities and Distribution of Pollutant Crude Oil. *Environ. pollut.* 2 (2), 97–113. doi: 10.1016/0013-9327(71)90014-0

Goldberg, E. D. (1963). "Geochronology With 210Pb," in *Radioactive Dating* (Vienna: . International Atomic Energy Agency), 121–131.

Goldschmidt, V. M. (1926). The Laws of Crystal Chemistry. *Naturwissenschaften* 14, 477–485. doi: 10.1007/BF01507527

Gorsline, D. S. (1996). Depositional Events in Santa Monica Basin, California Borderland, Over the Past Five Centuries. *Sedimentary Geol.* 104, 73–88. doi: 10.1016/0037-0738(95)00121-2

Grottoli, A. G. and Eakin, C. M. (2007). A Review of Modern Coral δ^{18}o and Δ^{14}C Proxy Records. *Earth-Science Rev.* 81, 67–91. doi: 10.1016/j.earscirev.2006.10.001

Hendy, I. L., Dunn, L., Schimmelmann, A. and Pak, D. K. (2013). Resolving Varve and Radiocarbon Chronology Differences During the Last 2000 Years in the Santa Barbara Basin Sedimentary Record, California. *Quat. Int.* 310, 155–168. doi: 10.1016/j.quaint.2012.09.006

Hendy, I. L. and Napier, T. J. Schimmelmann, A. (2015). From Extreme Rainfall to Drought: 250 Years of Annually Resolved Sediment Deposition in Santa Barbara Basin, California. *Quaternary Int.*387, 3–12. doi: 10.1016/j.quaint.2015.01.026

Heusser, L. (1998). Direct Correlation of Millennial-Scale Changes in Western North American Vegetation and Climate With Changes in the California Current System Over the Past ~60 Kyr. *Paleoceanography* 13, 252–262. doi: 10.1029/98PA00670

Hornafius, J. S., Quigley, D. and Luyendyk, B. P. (1999). The World's Most Spectacular Marine Hydrocarbon Seeps (Coal Oil Point, Santa Barbara Channel, California): Quantification of Emissions. *J. Geophys. Res.* 104, 20703–20711. doi: 10.1029/1999JC900148

Hua, Q., Barbetti, M. and Rakowski, A. Z. (2013). Atmospheric Radiocarbon for the Period 1950-2010. *Radiocarbon* 55, 2059–2072. doi: 10.2458/azu_js_rc.v55i2.16177

Ingram, B. L. and Kennett, D. J. (1995). Radiocarbon Chronology and Planktonic–Benthic Foraminifera ^{14}C Age Differences in Santa Barbara Basin Sediments, Hole 893A. *Proc. Ocean. Drill. Program Sci. Results* 146 (Pt. 2), 19–27. doi: 10.2973/odp.proc.sr.146-2.278.1995

Ingram, B. L. and Southon, J. R. (1996). Reservoir Ages in Eastern Pacific Coastal and Estuarine Waters. *Radiocarbon* 38, 573–582. doi: 10.1017/S0033822200030101

Inman, D. L. and Jenkins, S. A. (1999). Climate Change and the Episodicity of Sediment Flux of Small California Rivers. *J. Geol.* 107, 251–270. doi: 10.1086/314346

Jacox, M. G., Fiechter, J., Moore, A. M. and Edwards, C. A. (2015). ENSO and the California Current Coastal Upwelling Response. *J. Geophys. Research: Oceans* 120, 1691–1702. doi: 10.1002/2014JC010650

Kennett, D. J. and Brassell, S. C. (1992). Molecular Records of Twentieth Century El Niño Events in Laminated Sediments From Santa Barbara Basin. *Nature* 357, 62–64. doi: 10.1038/357062a0

Kennett, J. P. and Ingram, B. L. (1995). A 20,000 Year Record of Ocean Circulation and Climate Change From the Santa Barbara Basin. *Nature* 377, 510–514. doi: 10.1038/377510a0

Kennett, D. J., Ingram, B. L., Erlandson, J. M. and Walker, P. (1997). Evidence for Temporal Fluctuations in Marine Radiocarbon Reservoir Ages in the Santa Barbara Channel, Southern California. *J. Archaeolog Sci.* 24, 1051–1059. doi: 10.1006/jasc.1996.0184

Kim, J. C., Park, J. H., Kim, I. C., Lee, C., Cheoun, M. K., Kang, J., et al. (2001). Progress at the Seoul National University AMS Facility. *J. Korean Phys. Soc.* 39 (4), 23–35. doi: 10.1017/S0033822200037966

Kolpack, R. L. and Drake, D. E. (1984). Transport of Clays in the Eastern Part of Santa-Barbara Channel, California. *Geo-Mar. Lett.* 4, 191–196. doi: 10.1007/BF02281704

Kuo, T.-S., Liu, Z.-Q., Li, H.-C., Wan, N.-J., Shen, C.-C. and Ku, T.-L. (2011). Climate and Environmental Changes During the Past Millennium in Central Western Guizhou Reflected by Stalagmite ZJD-21 Record. *J. Asian Earth Sci.* 40, 1111–1120. doi: 10.1016/j.jseaes.2011.01.001

Lange, C. B., Berger, W. H., Burke, S. K., Casey, R. E., Schimmelmann, A., Soutar, A., et al. (1987). El Niño in Santa Barbara Basin: Diatom, Radiolarian and Foraminiferan Responses to the "1983 El Niño" Event. *Mar. Geol.* 78, 153–160. doi: 10.1016/0025-3227(87)90074-0

Li, H.-C., Ku, T.-L., Chen, W.-J., Jiao, W.-Q., Zhao, S.-S., Chen, T.-M., et al. (1996). Isotope Studies of Shihua Cave, Beijing – II: Radiocarbon Dating and Age Correction of Stalagmite. *Seismol. Geol.* 18, 329–338.

Li, H.-C., Lee, Z.-H., Wan, N.-J., Shen, C.-C., Li, T.-Y., Yuan, D.-X., et al. (2011). Interpretations of ^{18}O and ^{13}C in Aragonite Stalagmites From Furong Cave, Chongqing, China: A 2000-Year Record of Monsoonal Climate, J. *Asian Earth Sci.* 40, 1121–1130. doi: 10.1016/j.jseaes.2010.06.011

Li, C., Sessions, A. L., Kinnaman, F. S. and Valentine, D. L. (2009). Hydrogen-Isotopic Variability in Lipids From Santa Barbara Basin Sediments. *Geochimica. Cosmochimica. Acta* 73 (16), 4803–4823. doi: 10.1016/j.gca.2009.05.056

Li, H.-C., Zhao, M., Tsai, C.-H., Mii, H.-S. and Wei, K.-Y. (2015). The First High-Resolution Stalagmite Record From Taiwan: Climate and Environmental Changes During the Past 1300 Years. *J. Asian Earth Sci.* 114, 574–587. doi: 10.1016/j.jseaes.2015.07.025

Löwemark, L.Itrax operators (2019). Practical Guidelines and Recent Advances in the Itrax XRF Core-Scanning Procedure. *Quaternary Int.* 514, 16–29. doi: 10.1016/j.quaint.2018.10.044

Lund, D. C. (2011). Increased Ventilation Age of the Deep Northeast Pacific Ocean During the Last Deglaciation. *Nat. Geosci.* 4, 771–774. doi: 10.1038/ngeo1272

Lynn, R. J. and Bograd, S. J. (2002). Dynamic Evolution of the 1997–1999 El Niño–La Niña Cycle in the Southern California Current System. *Prog. Oceanogr.* 54 (1-4), 59–75. doi: 10.1016/S0079-6611(02)00043-5

Lynn, R. J. and Simpson, J. J. (1990). The Flow of the Undercurrent Over the Continental Borderland Off Southern California. *J. Geophys. Res.* 95 (C8), 12,995–13,008. doi: 10.1029/JC095iC08p12995

McFadgen, B. and Manning, M. R. (1990). Calibrating New Zealand Radiocarbon Dates of Marine Shells. *Radiocarbon* 32 (2), 229–232. doi: 10.1017/S0033822200040194

McGowan, J. A. (1984). The California El Niño 1983. *Oceanus* 27 (2), 5–12.

Napier, T. J., Hendy, I. L., Fahnestock, M. F. and Bryce, J. G. (2019). Provenance of Detrital Sediments in Santa Barbara Basin, California, USA: Changes in Source Contributions Between the Last Glacial Maximum and Holocene. *GSA Bull.* 132 (1–2), 65–84. doi: 10.1130/B32035.1

Paulsen, D. E., Li, H.-C. and Ku, T.-L. (2003). Climate Variability in Central China Over the Last 1270 Years Revealed by High-Resolution Stalagmite Records. *Quat. Sci. Rev.* 22, 691–701. doi: 10.1016/S0277-3791(02)00240-8

Pisias, N. G. (1978). Paleoceanography of the Santa Barbara Basin During the Last 8000 Years. *Quaternary Res.* 10, 366–384. doi: 10.1016/0033-5894(78)90027-3

Ramage, C. S. (1986). El Niño. *Am. Scientist* 254, 77–83.

Rassmusson, E. M. (1984). El Niño: The Ocean/Atmosphere Connection. *Oceanus* 27 (2), 5–12.

Roark, E. B., Ingram, B. L., Southon, J. R. and Kennett, J. P. (2003). Holocene Foraminiferal Radiocarbon Record of Paleocirculation in the Santa Barbara Basin. *Geology* 31, 379–382. doi: 10.1130/0091-7613(2003)031<0379:HFRROP>2.0.CO;2

Robert, C. (2004). Late Quaternary Variability of Precipitation in Southern California and Climatic Implications: Clay Mineral Evidence From the Santa Barbara Basin, ODP Site 893. *Quat. Sci. Rev.* 23, 1029–1040. doi: 10.1016/j.quascirev.2003.11.005

Ropelewski, C. F. and Jones, P. D. (1987). An Extension of the Tahiti-Darwin Southern Oscillation Index. *Monthly Weather Rev.* 115, 2161–2165. doi: 10.1175/1520-0493(1987)115<2161:AEOTTS>2.0.CO;2

Sarno, C. T., Benitez-Nelson, C. R., Ziolkowski, L. A., Hendy, I. L., Davis, C. V., Tappa, E. J., et al. (2020). The Impacts of Flood, Drought, and Turbidites on Organic Carbon Burial Over the Past 2,000 Years in the Santa Barbara Basin. *California Paleoceanogr. Paleoclimatol.* 35 (7), e2020PA00384. doi: 10.1029/2020PA003849

Schimmelmann, A., Hendy, I. L., Dunn, L., Pak, D. K. and Lange, C. B. (2013). Revised ~2000-Year Chronostratigraphy of Partially Varved Marine Sediment in Santa Barbara Basin, California. *GFF* 135 (3–4), 258–264. doi: 10.1080/11035897.2013.773066

Schimmelmann, A. and Lange, C. B. (1992). Extreme Climatic Conditions Recorded in Santa Barbara Basin Laminated Sediments: The 1835-1840 Macoma Event. *Mar. Geol.* pp, 279–299. doi: 10.1016/0025-3227(92)90134-4

Schimmelmann, A. and Lange, C. B. (1996). Tales of 1001 Varves: A Review of Santa Barbara Basin Sediment Studies. *Geolog. Soc. London Special Publications* 116, 121–141. doi: 10.1144/GSL.SP.1996.116.01.12

Schimmelmann, A., Lange, C. B. and Li, H.-C. (2001). Major Flood Events of the Past 2,000 Years Recorded in Santa Barbara Basin Sediment. *Paclim. Conf. Proc.* pp, 82–103.

Schimmelmann, A., Lange, C. B. and Meggers, B. J. (2003). Palaeoclimatic and Archaeological Evidence for a 200-Yr Recurrence of Floods and Droughts Linking California, Mesoamerica and South America Over the Past 2000 Years. *Holocene.* 13 (5), 763–778. doi: 10.1191/0959683603hl661rp

Schimmelmann, A., Lange, C. B., Roark, E. B. and Ingram, B. L. (2006). Resources for Paleoceanographic and Paleoclimatic Analysis: A 6,700-Year Stratigraphy and Regional Radiocarbon Reservoir-Age (ΔR) Record Based on Varve Counting and ^{14}C-AMS Dating for the Santa Barbara Basin, Offshore California, U.S.A. *J. Sediment. Res.* 76, 74–80. doi: 10.2110/jsr.2006.04

Schimmelmann, A. and Tegner, M. J. (1991). Historical Oceanographic Events Reflected in ^{13}C/^{12}C Ratio of Total Organic Carbon in Laminated Santa Barbara Basin Sediment. *Global biogeochem. cycles* 5, 173–188. doi: 10.1029/91GB00382

Schimmelmann, A., Zhao, M., Harvey, C. C. and Lange, C. B. (1998). A Large California Flood and Correlative Global Climatic Events 400 Years Ago. *Quaternary Res.* 49 (1), 51–61. doi: 10.1006/qres.1997.1937

Schimmelmann, A., Zhao, M., Kuhn, G. G. and Tegner, M. J. (1995). "Sea Surface Temperature and Paleo-El Niño Events in Santa Barbara Basin, AD 1841-1941," in *Proceedings of the Eleventh Annual Pafic Climate (PACLIM) Workshop, April 19-22, 1994. Interagency Ecological Program. Technical Report 40.* Eds. Isaacs, C. M. and Tharp, V. L. (California Department of Water Resources), 93–105.

Shipe, R. F., Passow, U., Brzezinski, M. A., Graham, W. M., Pak, D. K., Siegel, D. A., et al. (2002). Effects of the 1997–98 El Niño on Seasonal Variations in Suspended and Sinking Particles in the Santa Barbara Basin. *Prog. Oceanogr.* 54, 105–127. doi: 10.1016/S0079-6611(02)00045-9

Stenström, K. E., Skog, G., Georgiadou, E., Genberg, J. and Johansson, A. (2011). "A Guide to Radiocarbon Units and Calculations," in *Internal Report LUNFD6(NFFR-3111)/1-17/(2011), Division of Nuclear Physics* (Sweden: Department of Physics, Lund University).

Stuiver, M. and Polach, H. A. (1977). Discussion/Reporting of ^{14}C Data. *Radiocarbon* 19, 355–363. doi: 10.1017/S0033822200003672

Tems, C. E., Berelson, W. M. and Prokopenko, M. G. (2015). Particulate δ^{15}n in Laminated Marine Sediments as a Proxy for Mixing Between the California Undercurrent and the California Current: A Proof of Concept. *Geophys. Res. Lett.* 42, 419–427. doi: 10.1002/2014GL061993

Thunell, R. C. (1998). Particle Fluxes in a Coastal Upwelling Zone: Sediment Trap Results From Santa Barbara Basin, California. *Deep-Sea Res. Part Ii-Topical Stud. Oceanogr.* 45, 1863–1884. doi: 10.1016/S0967-0645(98)80020-9

Thunell, R. C. (2003). Distinguishing Between Water Column and Sedimentary Denitrification in the Santa Barbara Basin Using the Stable Isotopes of Nitrate. *Geochem. Geophys. Geosyst.* 4 (5), 1040. doi: 10.1029/2002gc000384

Thunell, R. C., Tappa, E. and Anderson, D. M. (1995). Sediment Fluxes and Varve Formation in Santa Barbara Basin, Offshore California. *Geology* 23, 1083–1086. doi: 10.1130/0091-7613(1995)023<1083:SFAVFI>2.3.CO;2

Treude, T. and Ziebis, W. (2010). Methane Oxidation in Permeable Sediments at Hydrocarbon Seeps in the Santa Barbara Channel, California. *Biogeosciences* 7, 3095–3108. doi: 10.5194/bg-7-3095-2010

Valentine, D. L., Reddy, C. A., Farwell, C., Hill, T. M., Pizarro, O., Yoerger, D. R., et al. (2010). Asphalt Volcanoes as Potential Source of Methane to Late Pleistocene Coastal Waters, Nat. *Geosci.* 3, 345–348. doi: 10.1038/NGEO848

van Geen, A. and Husby, D. M. (1996). Cadmium in the California Current System: Tracer of Past and Present Upwelling. *J. Geophys. Res. (Oceans)* 101, 3489–3507. doi: 10.1029/95JC03302

Venrick, E. L. (2012). Phytoplankton in the California Current System Off Southern California: Changes in a Changing Environment. *Prog. Oceanogr.* 104, 46–58. doi: 10.1016/j.pocean.2012.05.005

Warrick, J. A. and Farnsworth, K. L. (2009). "Sources of Sediment to the Coastal Waters of the Southern California Bight," in *Earth Science in the Urban Ocean: The Southern California Continental Borderland, Geological Society of America Special Paper*, vol. 454 . Eds. Lee, H. J. and Normark, W. R., 39–52). doi: 10.1130/2009.2454(2.2

Warrick, J. A., Washburn, L., Brzezinski, M. A. and Siegel, D. A. (2005). Nutrient Contributions to the Santa Barbara Channel, California, From the Ephemeral Santa Clara River. *Estuarine Coast. Shelf Sci.* 62 (4), 559–574. doi: 10.1016/j.ecss.2004.09.033

Weinheimer, A. L. and Cayan, D. R. (1997). Radiolarian Assemblages From Santa Barbara Basin Sediments: Recent Interdecadal Variability. *Paleoceanography* 12, 658–670. doi: 10.1029/97PA00986

White, M. E., Rafter, P. A., Stephens, B. M., Wankel, S. D. and Aluwihare, L. I. (2019). Recent Increases in Water Column Denitrification in the Seasonally Suboxic Bottom Waters of the Santa Barbara Basin. *Geophys. Res. Lett.* 46, 6786–6795. doi: 10.1029/2019GL082075

Yang, Q. N., Zhao, H. Y., Li, H.-C., Li, H. K., Bu, Z. J., Wang, S. Z., et al. (2017). Distributions of "Bomb ^{14}C", Biogeochemistry and Elemental Concentration in Hani Mire Peat Profiles, NE China: Implications of Environmental Change. *Quat. Int.* 447, 128–143. doi: 10.1016/j.quaint.2017.06.033

Yin, J. J., Li, H.-C., Rao, Z.-G., Shen, C.-C., Mii, H.-S., Pillutla, R. K., et al. (2017). Variations of Monsoonal Rain and Vegetation During the Past Millennium in Tiangui Mountain, North China Reflected by Stalagmite δ^{18}O and δ^{13}C Records From Zhenzhu Cave. *Quaternary Int.* 447, 89–101. doi: 10.1016/j.quaint.2017.06.039

Yin, J. J., Li, H.-C., Tang, W., Wang, Z. J., Mii, H.-S. and Lin, Y. S. (2019). Rainfall Variability and Vegetation Recovery in Rocky Desertification Areas Recorded in Recently-Deposited Stalagmites From Guilin, South China. *Quaternary Int.* 528, 109–119. doi: 10.1016/j.quaint.2019.01.039

Yin, J. J., Yuan, D. X., Li, H.-C., Cheng, H., Li, T. Y., Edwards, R. L., et al. (2014). Variation in the Asian Monsoon Intensity and Dry–Wet Condition Since the Little Ice Age in Central China Revealed by an Aragonite Stalagmite. *Clim. Past* 10, 1803–1816. doi: 10.5194/cp-10-1803-2014

Zhao, M., Li, H.-C., Liu, Z.-H., Mii, H.-S., Sun, H.-S. and Shen, C.-C. (2015). Changes in Climate and Vegetation of Central Guizhou in Southwest China Since the Last Glacial Reflected by Stalagmite Records From Yelang Cave. *J. Asian Earth Sci.* 114, 549–561. doi: 10.1016/j.jseaes.2015.07.021

Zhao, M., Li, H.-C., Shen, C.-C., Kang, S.-C. and Chou, C.-Y. (2017a). δ^{18}O, δ^{13}C, Elemental Content and Depositional Features of a Stalagmite From Yelang Cave Reflecting Climate and Vegetation Changes Since Late Pleistocene in Central Guizhou, China. *Quaternary Int.* 452, 102–115. doi: 10.1016/j.quaint.2016.07.022

Zhao, M., Shen, G.-J., He, J.-N., Cao, B. and Li, H.-C. (2017b). AMS ^{14}C Dating of the Hominin Archaeological Site Chuandong Cave in Guizhou Province, Southwestern China. *Quaternary Int.* 447, 102–110. doi: 10.1016/j.quaint.2017.04.037

Conflict of Interest: The authors declare that the research was conducted in the absence of any commercial or financial relationships that could be construed as a potential conflict of interest.